Review

Development of metal matrix composites by laser-assisted additive manufacturing technologies: a review

Jing Shi[1,*] and Yachao Wang[1]

[1] Department of Mechanical and Materials Engineering, College of Engineering and Applied Science, University of Cincinnati, Cincinnati, OH 45221, USA

ABSTRACT

Metal matrix composites (MMCs) generally possess superior properties than the monotonic matrix alloys, and thus, they have become excellent candidate materials in various applications. Also, the ability of property tailoring at an affordable cost is of particular importance to industries. Among the many manufacturing techniques for MMCs, laser-assisted additive manufacturing (AM) techniques have emerged and drawn increasing attention in the past decade. In the literature, a wealth of studies have been carried out on the synthesis of MMCs via laser-assisted AM techniques, as well as the property evaluation of the obtained MMCs. In this paper, we review and analyze the relevant literature and summarize the material preparation, optimization of process parameters, resultant improvements, and corresponding strengthening mechanisms for each major category of MMCs. Moreover, the limitations and challenges related to MMC synthesis using the laser-assisted AM techniques are discussed, and the future research directions are suggested to address those issues.

Introduction

Metal matrix composites are usually comprised of a metallic matrix phase and at least one more constituent phase for reinforcing purpose. The reinforcement can be ceramics, carbon materials, or other metallic materials, in the form of particulates, platelets, whiskers, or fibers. For decades of years, MMCs have attracted considerable attention in aerospace, automotive, and other structural applications, as a result of their cost-effectiveness, enhanced mechanical and physical properties, as well as property-tailoring capability, compared to conventional monolithic metal alloys [1, 2]. The interest in MMCs began in the late 1950s, with limited development and applications in the aerospace field. In the 1960s, ceramic whiskers as discontinuous reinforcement in metals were studied for high-temperature applications in aircraft engines. Later in the 1970s and 1980s, automotive industries started to take MMCs into applications extensively [3]. In the past two decades, MMCs have experienced unprecedented growth thanks to the developments in materials and manufacturing technologies. Meanwhile, extensive

Address correspondence to E-mail: jing.shi@uc.edu

Springer

research has been conducted to characterize the mechanical behaviors and corresponding mechanisms of MMCs that lead to significantly enhanced strength, stiffness, and weight saving. Various combinations of reinforcements and matrix materials have been reported in the literature, while the focus has been on aluminum-, copper-, iron-matrix, nickel- and titanium-matrix composites, and the most frequently adopted reinforcement materials include carbides, nitrides, oxides, and so forth [4]. Without any doubt, MMCs still possess enormous potentials for scientific research as well as commercial applications.

Traditional manufacturing is often based on multi-stage processes, with the initial stage dealing with the rough part creation and the subsequent stages for material removal operations. Creating a rough metallic part from the raw material and later removing most of its volume may not be cost-effective. Moreover, the various stages of manufacturing often take place in different locations, which creates logistics issues and incurs more energy consumption. On the other hand, additive manufacturing (AM) technologies are able to build fully functional parts in a single operation, with minimum waste of materials. AM technologies also empower design engineers with more freedom to create the complex geometrical entities without worrying about the manufacturability issue. The Wohlers Report 2019 [5] indicates that the revenue of metal AM continues a 5-year streak of more than 40% growth each year. It also forecasts that the revenue of entire AM market will climb to $23.9 billion in 2022 and $35.6 billion in 2024. Industry is becoming aware of the benefits of producing metal parts by additive manufacturing.

In the past three decades, laser-assisted AM techniques have drawn significant attention from both academia and industry. They are now regarded as increasingly important manufacturing methods with growing niche areas of applications. A typical laser-assisted AM technique employs a laser beam to manufacture a part by fusing metal powders in a layer-by-layer manner based on the sliced 3D digital data containing the part geometry. Due to the market strategies of various companies in the additive manufacturing field, there exist many different names used for very similar additive manufacturing processes. Based on the terminologies defined by ASTM Standard F2792 [6], the metal AM processing methods can mainly be classified into two categories.

The first type is directed energy deposition (DED), in which focused thermal energy is used to fuse materials by melting as the materials are being deposited. DED bears several names, such as LENS (laser engineered net shaping) and LMD (laser metal deposition). The DED-type additive manufacturing owns the advantages of fast build rate, flexible powder composition, and capability of deposition on curved surfaces, and so on. The second type is powder bed fusion (PBF), in which thermal energy is used to selectively fuse powders in a powder bed. PBF includes several variants such as selective laser sintering (SLS), direct metal laser sintering (DMLS), and selective laser melting (SLM). The main advantages of PBF include high accuracy, surface quality, and often high mechanical properties. It is generally accepted that those advantages are attributed to small laser focus spot and the resulted fine microstructure and high resolution [7]. In this review, research works are organized according to the material classification of MMCs. In each group of MMCs, the laser-assisted AM techniques that have been adopted and performance enhancements that have been achieved are summarized and analyzed. Furthermore, the challenges and the future research directions on MMCs using laser-assisted AM are pointed out.

Aluminum-based metal matrix composites

Aluminum (Al) based materials are the second most used engineering material group after steels [8]. The low melting temperature of aluminum and its good bonding between a wide variety of reinforcements make Al-based alloys an ideal type of metal matrix material. Extensive studies on Al/Al alloy matrix-based composites have been reported in the literature, and the investigated reinforcement materials mainly include ceramic and carbon particles. Most of the existing studies on using laser-assisted AM to fabricate Al-based MMCs adopt the external second phase ceramic particles as reinforcements, which are economically viable. Generally, the external second phase particles bring certain strengthening effect but sacrifice in material ductility, due to dispersion difficulty, detrimental phase formation, and reduced powder flowability [9]. The investigation of these fundamental issues has been insufficient. On the other hand, the incorporation of carbon
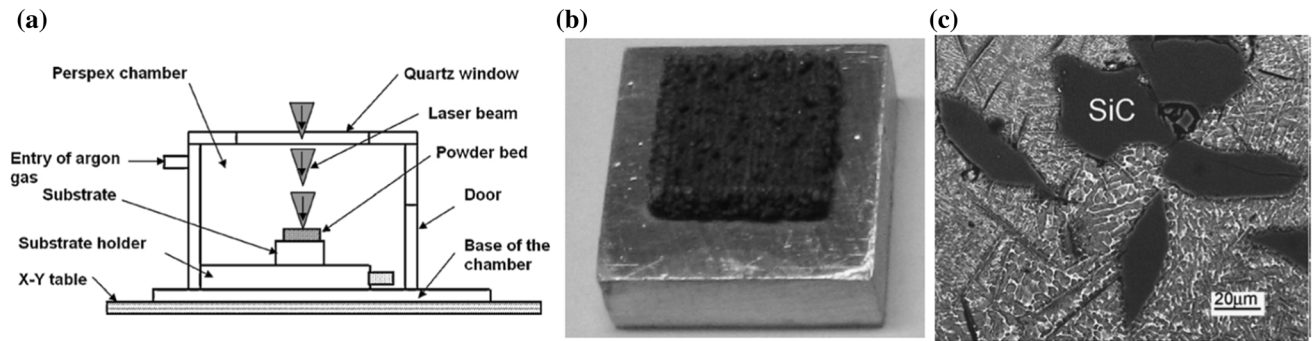
(a)

(b)

(c)

Figure 1 Al–4.5Cu–3Mg composite reinforced by SiC in the SLS process: **a** machine setup schematic, **b** as-built composite, and **c** SEM image showing the SiC particles [12].

nanomaterials, such as carbon nanotube or graphene, can significantly increase the material strength due to their excellent load-transfer effect [10]. However, the effective preservation of the structural integrity of carbon materials is a major challenge as the carbon elements tend to react with the metal matrix to form carbide, especially in the laser-induced high-temperature molten metals [11].

Reinforced by SiC particles

Ghosh et al. [12] use the DMLS method to manufacture SiC-reinforced Al–4.5Cu–3Mg MMC. The bonding between SiC particulates and the matrix alloy is smooth and free of cracks, as shown in Fig. 1. Also, the addition of 300 mesh size particles brings the optimum density, while the addition of 1200 mesh size particles generates the optimum microhardness. Also, the wear characteristics of DMLS-processed Al-MMCs are investigated under various combinations of size and volume fraction of SiC particles. It is found that the wear resistance of synthesized materials drops when the size of reinforcement particles increases, and crack density due to thermal stress of contraction stress increases after the volume percentage of reinforcement reaches 15%. Simchi and Godlinski [13] show that the densification rate of Al–7Si–0.3Mg/SiC composite in the laser sintering process obeys first-order kinetics and is significantly affected by SiC fractions. Also, Al_4SiC_4 is formed as a result of reaction between the aluminum melt and reinforcement particles. Similarly, in the DMLS process of Al–7Si–0.3Mg, Manfredi et al. [14] adopt two different ceramic reinforcement particles, namely, 10 wt% SiC and 1 wt% nano-sized $MgAl_2O_4$. The results show that in the case of SiC-reinforced MMC, the well-dispersed SiC particles completely react with

the matrix and form aluminum carbides, which lead to the hardness increase by 70%. However, in the case of nano-$MgAl_2O_4$-reinforced MMC, the hardness decreases by 11% owing to the high inhomogeneity of nano-reinforcement particles and high residual porosity. Another study also indicates that SiC particles react with AlSi10Mg matrix, and this leads to an in situ formation of micron-sized Al_4SiC_4 [15].

Reinforced by TiC particles

In reinforcing AlSi10Mg with nano-TiC particles [16], the microhardness of reinforced AlSi10Mg can increase by up to 30% compared with the unreinforced AlSi10Mg with proper parameter settings of the SLM process. It is found that the TiC particles tend to aggregate in the interdendritic regions as shown in Fig. 2. When a higher LEPUL (laser energy per unit length) is used, the nanoparticles tend to form a ring-like structure because of the coarsening of dendrites. Meanwhile, some TiC particles react with the Al matrix to form Al_9Si and Mg_2Si, as shown by the XRD spectrum. In a study on SLM-produced nano-TiC particle-reinforced AlSi10Mg MMC [17], the addition of TiC reinforcement significantly lowers the coefficient of friction (COF) and wear rate. Balling phenomenon on the material surface and the generation of detrimental residual stress are believed to be associated with insufficient laser energy density. Laser deposition method has also been reported to produce TiC particles-reinforced aluminum matrix composite [18], and the wear performance of obtained composite shows a 10-factor improvement, i.e., the wear rate reduces from 7.6×10^{-3} to 0.88×10^{-3} mm^3 m^{-1}.
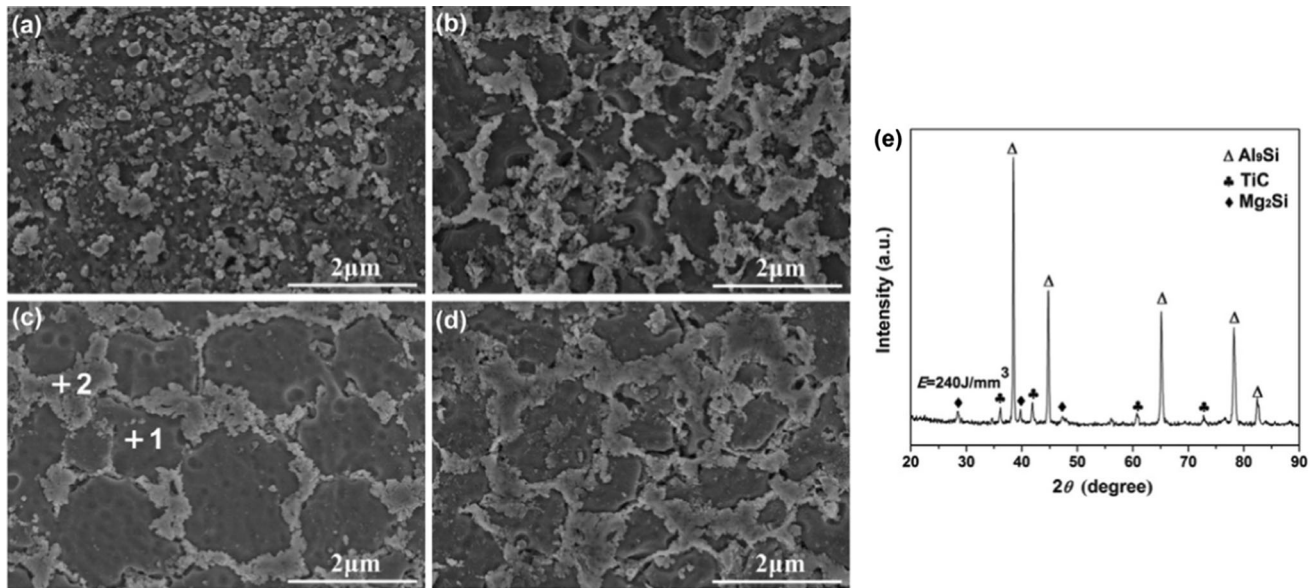
Figure 2 TiC/AlSi10 Mg MMCs prepared by SLM: **a–d** microstructures under laser energy densities of 160 J mm^{-3}, 200 J mm^{-3}, 240 J mm^{-3}, and 280 J mm^{-3}, respectively, and **e** XRD spectra showing the constituent phases of SLM-processed Al-based nanocomposites [16].

Reinforced by other types of ceramic particles

Other types of ceramic particles, such as Fe_2O_3, Al_2O_3, AlN, TiB_2, and SiC, have also been used to reinforce Al-based MMCs. Dadbakhsh and Hao [19] discover that HIP (hot isostatic pressing) does not efficiently densify the SLM-processed Al/5–15 wt% Fe_2O_3 material due to the existence of thick oxide bands formed between solids during the SLM process. The hardness also drops after HIP processing due to the annealing effect on material microstructure. A follow-up study is performed to investigate the influence of laser power and scanning speeds on the mechanical properties of the same composite material [20]. The results indicate the laser power is positively related to the surface roughness, but the relation of material density to laser powder is dependent upon the weight percentage of reinforcement. The addition of 4 vol% Al_2O_3 into Al during SLM significantly improves the yield strength by 36.3% and the hardness by 17.5% [21], as well as the ductility by more than 100%, as shown in Fig. 3. Sercombe et al. [22] use the SLS technique to fabricate an aluminum alloy preform, which is subsequently debound and infiltrated with a second aluminum alloy. The partial transformation of aluminum powders into a percolating AlN structure by reaction with nitrogen is achieved to form a rigid skeleton in the SLS process. This provides the structural support during the infiltration stage. A similar process is attempted by Yu and Schaffer [23], in which an aluminum alloy preform is first prepared by SLS, and then nitrided to form Al-AlN structure. The composite preform is then pressurelessly infiltrated by AA 6061 to achieve 100% improvement in density. For an AlN/AlSi10Mg composite system, the decrease in LEPUL from 1800 to 450 J/m results in a homogenous distribution of AlN particles [24]. Gas atomization is implemented to produce nano-TiB_2 decorated AlSi10Mg composite powder from a TiB_2/AlSi10Mg master casting ingot. The SLM-produced nTiB_2/AlSi10Mg exhibits superior strength and ductility that are higher than most conventionally fabricated wrought and tempered Al alloys [25]. In a SiC/AlSi10Mg composite fabricated by SLM [26], it is found that excessive filler content (over 10 wt%) leads to the prevalence of pores in the composite and triggers the formation of carbides.

Reinforced by carbon materials

Recently, carbon nanomaterials have also become an attractive option to reinforce aluminum and its alloys. The low processing temperature of aluminum helps preserve the structural integrity of carbon
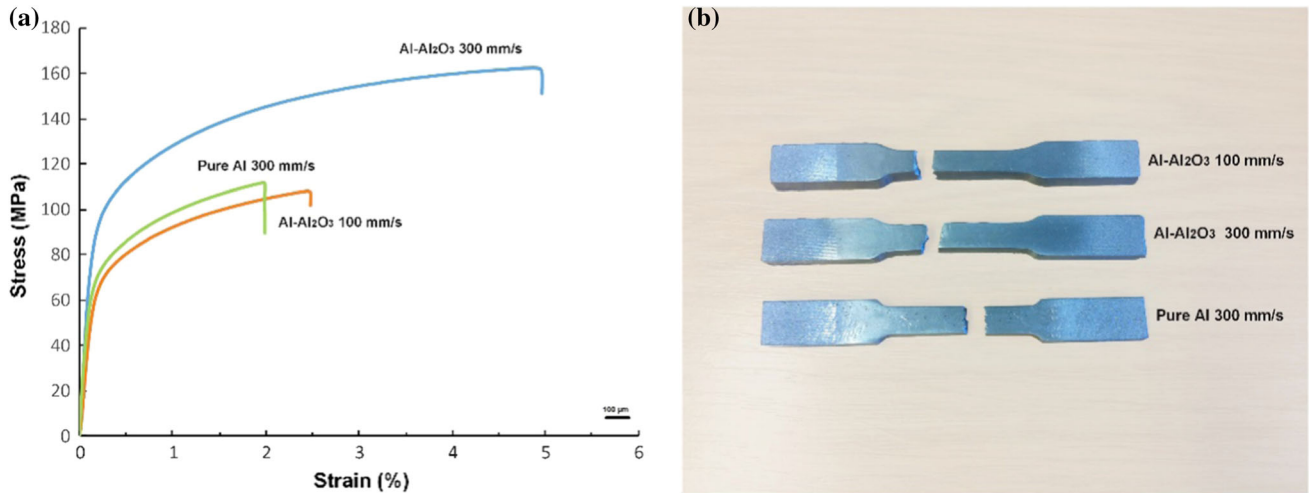
Figure 3 Tensile performance of Al–Al$_2$O$_3$ composite fabricated by SLM, **a** tensile curves and **b** fractured specimens. [21].

materials. For instance, carbon nanotubes (CNTs) have been used as reinforcement to strengthen the SLM-processed AlSi10Mg. With 1 wt% addition of CNTs, the hardness and the tensile strength increase by 10% and 20%, respectively [27]. As shown in Fig. 4, although some CNTs react with the AlSi10Mg matrix phase to generate aluminum carbides, many CNTs are found intact in the matrix and contribute to the high strength of the composite. The electrical resistivity is found to be significantly lower without the formation of common brittle Al$_4$C$_3$ phase [28]. Wang and Shi [29] apply SLM to synthesize graphene-reinforced AlSi10Mg composites. The strengthening effect of graphene is estimated to be
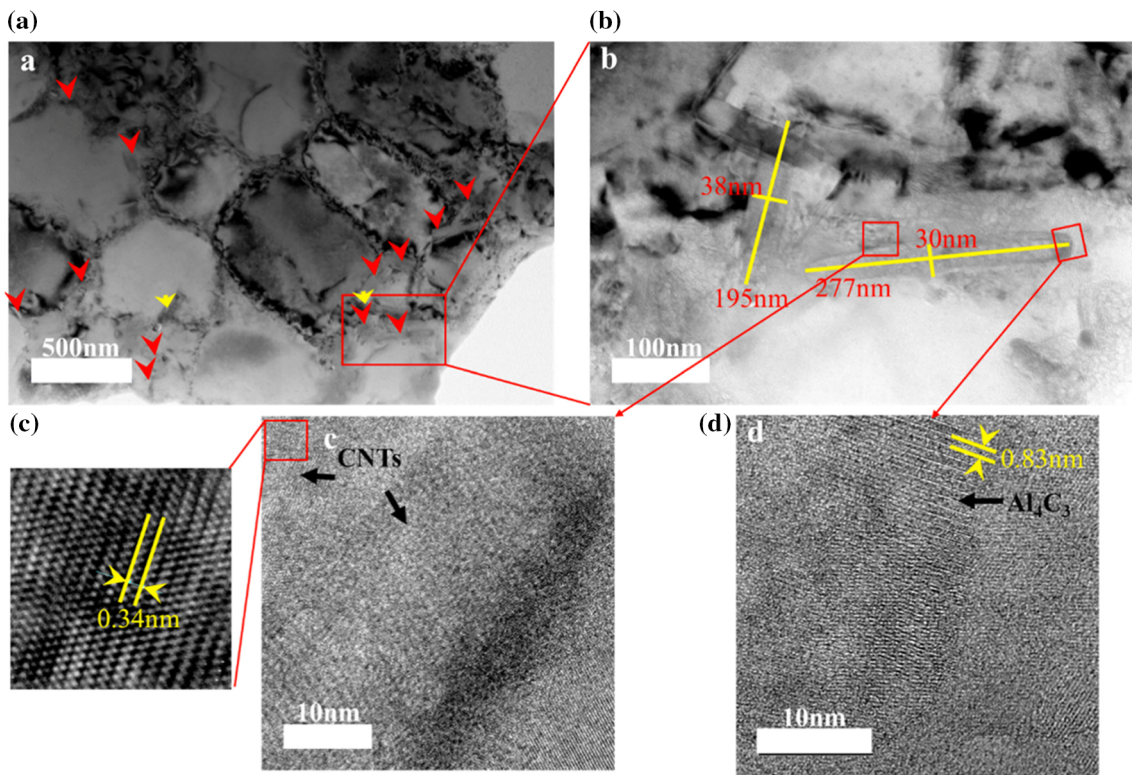

Figure 4 CNTs and reaction product in the SLM-produced AlSi10Mg. **a**, **b** TEM of CNTs in the test parts, wherein the yellow arrow indicates Al$_4$C$_3$ and the red indicates CNTs. **c**, **d** The high-resolution TEM images of CNTs in the test parts [27].

Table 1 Literature on Al/Al alloy matrix-based composites fabricated by laser-assisted additive manufacturing

Authors	Materials/preparation	Laser processing parameters	Effects/improvements/findings
Ghosh et al. [12]	Al–4.5Cu–3Mg (44 μm) and SiC (300–1200 mesh), volume ratio of SiC 10–30%	DMLS Laser pulse energy: 9 J Laser pulse width: 18 ms Layer thickness: 400 μm Scan spacing: 450 μm	300 mesh of SiC provides higher density Microhardness increases with the increase in SiC content Microhardness increases from less than 2–4 GPa, with addition of 30 vol% SiC particles
Simchi and Godlinski [13]	Pure Al (44 μm), AlMg10 (35 μm), Si (7 μm) to form Al7Si0.3Mg, 5–20 vol% SiC (6.5 μm)	SLS Laser intensity: 8.6 W mm^{-2} Layer thickness: 100 μm Scan spacing: 300 μm	In situ formed Al_4SiC_4 is found Addition of 5 vol% SiC particles increases the densification level of Al–7Si–0.3Mg SiC increases the stability and leads to better surface finish
Manfredi et al. [14]	Al7Si0.3Mg + 10 wt% SiC	DMLS Laser power: 180–195 W Scan speed: 500–700 mm/s Scan spacing: 170 μm	Residual porosity is 4.4–5% SiC almost disappears and Al_4C_3 is formed Hardness of the MMC is 70% higher than the pure AlSiMg by DMLS
	Al7Si0.3Mg 1 wt% nano-sized MgAl2O4	DMLS Laser power: 180–195 W Scan speed: 600–800 mm/s Scan spacing: 170 μm	Residual porosity is 2.2–3.5% In situ formation of intermetallic Mg_2Si and $AlSiO_x$ is observed Higher inhomogeneity and lower hardness are obtained compared to pure AlSiMg by DMLS
Gu et al. [16]	AlMg10 (30 μm) and 3 wt% TiC (50 nm)	SLM Laser power: 80–140 W Scan speed: 200 mm/s Layer thickness: 50 μm Scan spacing: 50 μm	Tensile strength increases to 486 MPa from 400 MPa (unreinforced), with uncompromised elongation of 10.9% Microhardness increases to 188.3 $HV_{0.1}$ from 145 $HV_{0.1}$ (unreinforced)
Dubourg et al. [18]	0–30 vol% TiC (50–150 μm) and Al–12Si (45–90 μm)	LMD Laser power: 1800 W Spot size: 3 mm Scan speed: 7–17 mm/s	The microstructure of deposited composite is free of cracks. Carbide reinforcement is uniformly distributed in the matrix The worn surface becomes homogeneous when 30 vol% TiC is added. The wear rate significantly reduces from 7.6×10^{-3} to 0.88×10^{-3} mm^3 m^{-1}
Dadbakhsh and Hao [19]	Pure Al (40 μm) and 5–15 wt% Fe_2O_3 (53 μm)	SLM Laser power: 70 W Scan speed: 0.25 m/s Layer thickness: 50 μm Scan spacing: 50 μm	HIP post-treatment alters the microstructure and mechanical performance of product HIP post-treatment eliminates non-stable phases in the composite (i.e., Al_2Fe, AlFe, Fe_3Al and intermediate-Al_2O_3) Microhardness after HIP treatment increases as the increase in Fe_2O_3 content
Dadbakhsh et al. [20]	Pure Al (40 μm) and 5–15 wt% Fe_2O_3 (53 μm)	SLM Laser power: 39-91 W Scan speed: 0.5–0.14 m/s Layer thickness: 50 μm Scan spacing: 50 μm	In situ reaction between Al and Fe_2O_3 releases extra heat to assist melting development and improve the SLM processability Increase in Fe_2O_3 increases the density and reduces surface roughness of the product
Han et al. [21]	Al_2O_3 (50 nm, 4 vol%) and Al	SLM Laser power: 200 W Layer thickness: 30 μm Scan speed: 100–600 mm/s Spot size: 70 μm Discrete point exposure	Fully dense parts are obtained under 317.5 J/mm^3 and 300 mm/s Adding 4 vol% Al_2O_3 leads to 36.3% increase in yield strength and 17.5% increase in microhardness Further cold working results in 39% increase in hardness

Table 1 continued

Authors	Materials/preparation	Laser processing parameters	Effects/improvements/findings
Sercombe et al. [22]	Mixture of AA6061 alloy powder, 2 wt% Mg and 4 wt% nylon. Post-treatment: Thermal treated at 570 °C for 6 h in N_2, then infiltrated with Al–14.8Si–4.2Mg at 570 °C for 6 h	SLS Laser power: 28 W	Formed AlN skeleton improves the dimensional stability during infiltration
Yu and Schaffer [23]	High-speed steel. Post-treatment: Infiltrated in AA6061 at 1060 °C for 3 h	SLS Laser power: 50 W Scan speed: 1 mm/s Scan spacing: 682 μm Layer thickness: 500 μm	Flexural strength increases from 250 to 631 MPa Flexural modulus increases from 79 to 123.7 GPa
Dai et al. [24]	AlN (0.3 μm) and AlSi10Mg (30 μm)	SLM Laser power: 200 W Spot size: 70 μm LEPUL: 450–1800 J/m	The distribution of AlN changes from severally agglomeration to homogeneous dispersion as LEPUL decreases from 1800 to 450 J/m
Li et al. [25]	Gas atomization from a master casting AlSi10Mg ingot containing TiB_2 (7 vol%, 100 nm). Atomized composite powder (15–45 μm by screening) for SLM	SLM Laser power: 200–300 W Scan speed: 800–2000 mm/s Layer thickness: 30 μm Scan spacing: 105 μm	Coherent bonding is found at $nTiB_2$/Al and Si/Al interfaces High tensile strength (530 MPa), ductility (15.5%), and microhardness (191 $HV_{0.3}$) are obtained
Famodimu et al. [26]	5–10 wt% SiC and AlSi10Mg (63 μm)	SLM Laser power: 195 W Scan distance: 0.5 mm Layer thickness: 0.3 μm	Near fully dense composite is obtained when 5 wt% SiC is added under low scan speed Higher scan speed (over 800 mm/s) leads to a prevalent formation of hydrogen pores High filler content (10 wt%) leads to the formation of carbides
Jiang et al. [27]	1 wt% CNTs (outer diameter 20–30 nm, inner diameter 5–10 nm, length 10–30 nm) and AlSi10Mg powder	SLM Laser power: 370 W Scan speed: 900–1900 mm/s Scan spacing: 105 μm Layer thickness: 30 μm	Some CNTs react with the matrix material to generate Al_4C_3 carbide The increases in hardness and strength are 10% and 20%, respectively, as compared to unreinforced parts
Zhao et al. [28]	AlSi10Mg (30 μm) and multi-walled CNTs (diameter 8–15 nm, length < 50 μm)	SLM Laser power: 240–360 W Scan speed: 550–750 mm/s Scan spacing: 80 μm Layer thickness: 30 μm	Due to gas trapped by CNTs, the material exhibits high porosity CNTs are decomposed No formation of brittle Al_4C_3 is observed Hardness is improved due to carbon dispersion Significant reduction in electrical resistivity is achieved
Wang and Shi [29]	0.5 wt% graphene (5–50 μm) and AlSi10Mg (30 μm)	SLM Laser power: 370 W Scan speed: 1300 mm/s Layer thickness: 30 μm	The strengthening effect of graphene reaches over 60 MPa Higher porosity is found in the matrix mainly due to poor flow ability of graphene in metal powder
Slocombe and Li [30]	TiO_2, Al, and C (all < 90 μm in size)	SLS Laser power: 60 W Scan speed: 2 mm/s	Starting powders react to generate TiC and Al_2O_3 Below a certain threshold, no reactions take place due to insufficient thermal energy

Table 1 continued

Authors	Materials/preparation	Laser processing parameters	Effects/improvements/findings
Ghosh and Saha [31]	Al–4.5Cu–3Mg (44 μm) and 10–30 vol% SiC (300–1200 mesh)	*DMLS* Laser pulse energy: 9 J Laser pulse width: 18 ms Layer thickness: 400 μm Scan spacing: 450 μm	Addition of SiCp higher than 15 vol% increases the crack density Increase in particle size reduces the wear performance Wear resistance no longer increases after 20 vol% of SiC

over 60 MPa. However, high porosity is observed in the composite due to the adverse effect of graphene nanoplates on powder flowability. Table 1 summarizes the materials, techniques, and experimental parameters of additively manufactured Al-based MMCs.

Copper-based metal matrix composites

Thanks to excellent high-temperature mechanical properties and thermal conductivity, many copper alloy materials have been widely used for critical components serviced in high temperature environments. The high chemical stability of copper also makes it an ideal material for laser-assisted additive manufacturing. Copper-based matrix composites have been fabricated with various reinforcing materials. Tungsten and tungsten carbides are the major type of reinforcing materials to reinforce copper in AM processes, mainly because of good chemical stability between copper and tungsten. Thanks to the high hardness of tungsten, this type of composite generally exhibits significantly enhanced hardness and wear performance. However, inferior ductility is obtained because of the brittle interface between copper and tungsten formed during rapid cooling [32]. In this regard, effective engineering of the matrix/reinforcement interface could potentially lead to a major breakthrough. Additionally, a wide variety of copper matrix composites can be manufactured through post-infiltration using molten copper, due to the relatively low melting point of copper. This method brings better matrix/reinforcement interface quality due to controllable slow cooling, but it requires a green part to be built first and then go through costly post-processing steps. Thus, it is believed that the efficient green part design and the development of fast infiltration technology are

necessary in the endeavors of further exploring the potential of copper-based composites.

Reinforced by tungsten/tungsten carbide

Pintsuk et al. [33] develop W/Cu functionally graded composite materials through laser metal deposition process and observe well-distributed W particles within Cu matrix. The product property is comparable to that obtained from another additive manufacturing method—plasma spraying. Gu and Shen [34] fabricate submicron WC–Co particulate-reinforced Cu matrix composite material by DMLS. Phase characterization of WC–Co particles indicates that reinforcement particles are partially dissolved and smoothened. Further research of the same material is carried out to understand the sintering and reinforcement mechanism during DMLS process [35], as well as the effects of DMLS process parameters and the weight fraction of WC–Co reinforcement. Interestingly, the influence of rare earth (RE) material addition on WC particle reinforce Cu composite by the DMLS process is also studied [36]. It is found that the addition of RE–Si–Fe significantly improves the mechanical properties of product, homogenizes the reinforcement particles by significantly reducing the surface tension of the melts in the pool and pining effect of liquid/solid-phase boundary. Similar findings are reported in the investigation of adding rare earth oxide La_2O_3 to DMLS-processed WC–Co-reinforced Cu material [37], as shown in Fig. 5.

Reinforced by nickel

Nickel is another efficient reinforcement for copper because of its good bonding wettability on copper. In this regard, nickel particles are usually mixed with the copper matrix particles to achieve strengthening effects. Agarwala et al. [38] produce bronze–nickel parts by SLS process, in which the raw martial used
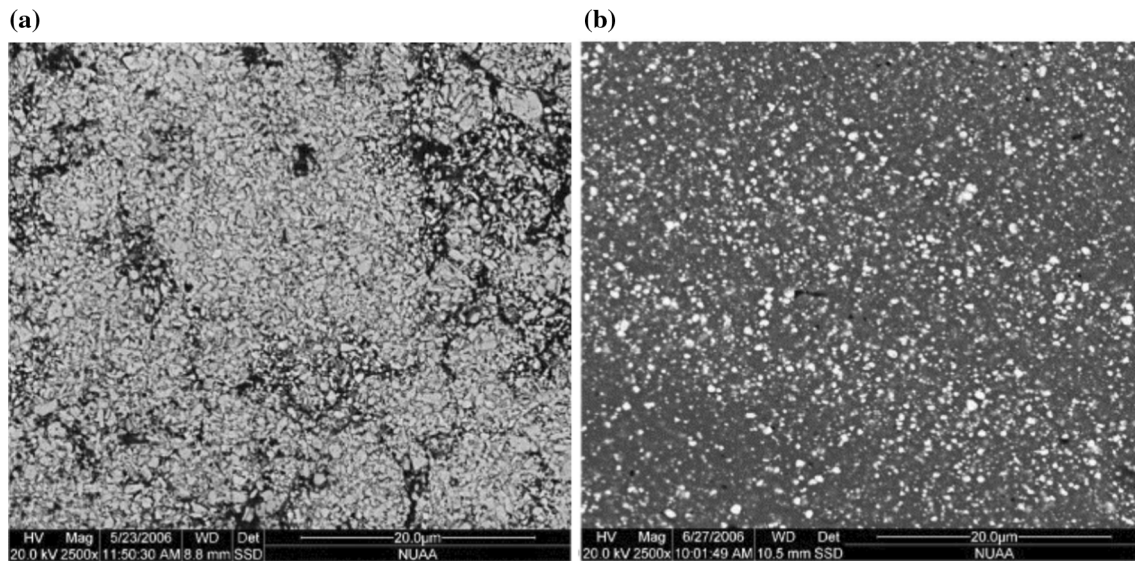
Figure 5 Addition of rear earth (RE) element effectively promotes the dispersion of WC powder in Cu matrix, **a** without RE addition and **b** with RE addition [37].

are bronze and nickel powder mixture. Ni particles are well preserved in the SLS green part. Liquid phase sintering as a post-processing is used on the SLS green part to increase the density and strength. The addition of Ni is found helpful to mitigate the high porosity issue in the composite material. Similarly, the DMLS process is employed to reinforce Cu matrix by Ni particles [39]. Full melting of matrix material and partial melting of reinforcing particles are the main sintering mechanism during the DMLS process. It is also discovered that the addition of phosphorus element acts as deoxidizer that limits the formation of copper oxide, and thus enhancing the liquid–solid wettability. In addition, Dürr et al. [40] fabricate EDM electrodes based on bronze–nickel powder mixture by means of SLS. The SLS EDM electrodes are infiltrated with silver, which leads to the improvement of wear performance by 30%.

Reinforced by in situ formation of ceramics

In situ formation of TiC is observed in the SLM process of Cu–Ti–C powder mixtures [41]. By adding Ni into the powder mixture, it is found that both microstructure and surface quality of SLM-produced product is improved. Similarly, in situ formation of TiB reinforcing particles is observed in the SLM process of Cu–Ti–B_4C powder mixture [42]. In the SLM process, the in situ reaction results in the

formation of TiB_2 and non-stoichiometric TiC_{1-x} particles in the Cu matrix.

Reinforced by carbon materials

A graphene-copper nanocomposite is fabricated by Hu et al. [43], in which the graphene is found to be intact in the copper matrix and the reinforced copper shows increases of 17.6% and 50% in average modulus and hardness, respectively. More recently, a feasibility study is carried out on additive manufacturing of metal-based cutting tool with incorporated diamond particles [44], in which Cu–Sn–Ti alloy powders with 10–20 vol% Ni-coated diamonds are SLM-processed. It is found that the majority of the diamonds can survive the SLM process and the diamond particles are well bonded to the matrix material.

Reinforced by infiltration materials

Cu/Cu alloy matrix-based composites can be obtained from a two-step approach, with the first step being laser-assisted additive manufacturing, and the second step being the post-processing to infiltrate a new type of material. In the study of Liu [45], the mixture of electrolytic Fe powder, deoxidized Cu powder, carbonyl Ni powder, graphite powder, and polymer binder powder is indirectly laser-sintered to
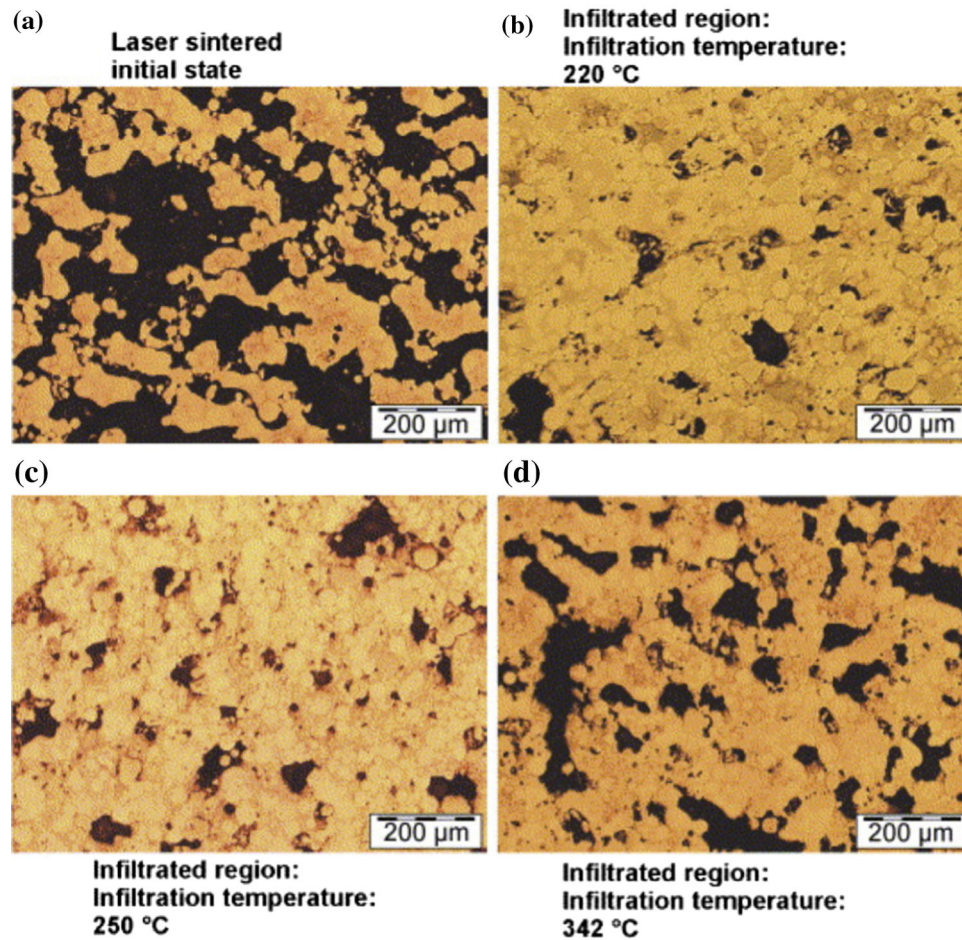
Figure 6 $Sn_{60}PbAg$ used as infiltrate material for bronze–nickel alloy produced by DMLS [46].

obtain Fe–Cu–Ni–C alloy. After being infiltrated in molten Cu, the Cu matrix Fe–Cu–Ni–C alloy composite is obtained and the relative density of the product is significantly increased. Pressure infiltration is adopted to reduce the porosity of bronze–nickel injection molds fabricated by DMLS [46]. The infiltrant used is $Sn_{60}PbAg$. It is discovered that residual porosity rises at higher infiltration temperatures because of the reduced capillary forces as well as the decreased infiltration depth, as shown in Fig. 6. Surface tension and pressure difference in the pores are found to be the most critical factors that impact infiltration performance. Meanwhile, due to its high viscosity and good wettability to metals, epoxy is adopted to post-treat the Cu-based alloy fabricated by laser-assisted additive manufacturing processes [47, 48]. Significant improvements on material

hardness, surface roughness, and average density are obtained. For the materials, techniques, and experimental parameters adopted in the above-mentioned studies on Cu/Cu alloy composites, we refer readers to Table 2 for further information.

Iron-based metal matrix composites

Iron is the most used metal material in the industry due to its low cost, stable chemical properties, balanced mechanical properties, and high compatibility with a wide range of alloying elements. Compared with nonferrous metals, iron-based alloys are relatively easier to produce due to the improved interaction with laser beam, higher energy absorptivity, lower reflection, and comparatively lower thermal

Table 2 Literature on Cu/Cu alloy matrix-based composites fabricated by laser-assisted additive manufacturing

Authors	Materials/preparation	Laser processing parameters	Effects/improvements/findings
Pintsuk et al. [33]	W (5.5 μm) and Cu (32 μm)	*SLS* Laser power: 2.5 kW	W particles are well distributed in Cu matrix
Gu and Shen [34]	Cu (15 μm) and WC–10%Co (0.6 μm), weight ratio 70:30	*DMLS* Laser power: 700 W Spot size: 0.3 mm Scan speed: 60 mm/s Scan spacing: 0.15 mm	WC reinforcing particulates are smoothened or completely dissolved Lowering the WC–Co amount results in insufficient reinforcement, while excessive WC–Co leads to agglomeration of WC particulates Homogenous sintered structure is obtained, with a high hardness of $HV_{0.1}384.6$
Gu et al. [36]	Cu (15 μm), WC (1.2 μm), and RE–Si–Fe (20 μm) weight ratio 60:37:3	*DMLS* Laser power: 700 W Spot size: 0.3 mm Scan speed: 50 mm/s Scan spacing: 150 μm Layer thickness: 200 μm	By adding RE–Si–Fe particles, the wettability between matrix/particle interfaces is improved, the WC reinforcing particles are refined, and their dispersion is homogenized RE–Si–Fe containing composite shows significantly elevated densification level (95.7%), microhardness (417.6 HV), fracture strength (201.8 MPa)
Gu et al. [37]	Cu (15 μm) and WC–10%Co (0.8 μm), weight ratio 80:20	*SLS* Laser power: 700 W Spot size: 0.3 mm Scan speed: 60 mm/s Scan spacing: 0.15 mm	Metastable phase $CoC_{0.25}$ is formed WC reinforcing particulates exhibit different morphologies Novel WC-core and Cu-coated structure is found Average hardness is $HV_{0.1}268.5$, and its value varies considerably due to segregation of WC
Gu et al. [37]	Cu (15 μm), WC (1.2 μm), and La_2O_3(20 μm) weight ratio 50:49:1	*DMLS* Laser power: 700 W Spot size: 0.3 mm Scan speed: 60 mm/s Scan spacing: 150 μm Layer thickness: 200 μm	Addition of RE La_2O_3 favors the microstructural refinement and improves the particulate dispersion homogeneity and the particulate/matrix interfacial coherence Addition of RE La_2O_3 decreases the surface tension of melt, resist grain growth coarsening Relative density is improved to 91.3% from 79% (without the addition of RE La_2O_3) Hardness is improved to 401 $HV_{0.1}$ from about 250 $HV_{0.1}$(without the addition of RE La_2O_3)
Agarwala et al. [38]	Cu–Sn powder (30–50 μm) and Ni (75–150 μm)	*SLS* Laser power: 35–56 W Scan speed: 0.2–1.5 in./s Scan spacing: 0.01–0.02 inch Layer thickness: 0.01–0.02 inch	Density and strength increase as the layer thickness decreases, scan speed decreases and laser power increases Post-sintering decreases the composite hardness due to the homogenization of bronze and Ni
Gu et al. [39]	Ni (52 μm), CuSn (10 wt% Sn, 28 μm), and CuP (8.4 wt% P) in weight ratio 60:30:10	*DMLS* Laser power: 600 W Layer thickness: 200 μm Scan speed: 40 mm/s Scan spacing: 150 μm	Significant smoothening of Ni occurs Dissolved Ni leads to improved particle/matrix interface Cu matrix mainly consists of CuNi and Cu_3Sn High theoretical density of 95.2% is obtained. Ni reinforcing phase has nanohardness of 1.82 GPa

Table 2 continued

Authors	Materials/preparation	Laser processing parameters	Effects/improvements/findings
Dürr et al. [40]	Bronze–nickel alloy Post-treatment: Infiltration by silver	*SLS* Laser power: 95 W Scan speed: 150 mm/s Scan spacing: 50 μm Layer thickness: 100 μm	Relative electrode wear reduces from 100 to 70% (pulse time 100 μs, pulsed current 12 A, and pulse break 10 μs) Porosity reduces from 32.3 to 2.3%
Lu et al. [41]	Cu, Ti, C, Ni powder mixture	*SLM* Laser power: 100 W Layer thickness: 200 μm	In situ TiC particles (less than 1 μm) are formed with the nominal composition of 40% Adding of Ni improves the wettability between Cu and TiC particles, and the melting behavior of Cu
Leong et al. [42]	Cu (30 μm), B_4C (2 μm), Ni (130 μm) and Ti (150 μm) Ti/B_4C weight ratio 3:1, Cu 80–95 wt%	*SLS* Laser power: 1000–2000 W Scan speed: 50–500 mm/min	In situ TiB_2 and TiC are formed By adding Ni, the interfacial integrity is greatly improved, and the porosity is reduced
Hu et al. [43]	COOH-rich nanoplatelets (diameter 10 μm and edge length 2 μm)	Indirection metal laser sintering (polyvinyl used for binder) Laser power: 70 W Scan speed: 2 mm/s Laser beam size: 0.8 mm	Graphene sheets are dispersed uniformly in the copper matrix Hardness increases by 22.7% with addition of graphene
Spierings et al. [44]	Cu–Sn–Ti–Zr alloy powder (20 μm), Ni-coated diamond particle (33 μm)	*SLM* Laser power: 100 W Laser spot: 0.2 mm Layer thickness: 30 μm Scan speed: 700–1100 mm/s Scan spacing: 0.09–0.11 mm	Stable specimens containing intact diamonds could be produced Cyclic heat impact on the diamond particles does not lead to graphitization Diamond particles are well bonded to matrix, and thin interfacial layer of TiC may be formed A relative density of over 98% is achieved
Liu et al. [45]	Bronze–nickel Post-treatment: Sintering at 1200 °C for 1 h (20 °C/h), then infiltrated by molten Cu at temperature 1200 °C for 40 min. Lastly thermal treatment at 930 °C for 1 h	*SLS* Laser power: 21 W Scan speed: 2000 mm/s Scan spacing: 100 μm Layer thickness: 100 μm	Cu and Ni diffuse into γ-Fe, Ni also diffuses into α-Cu. Cu precipitates at room temperature Yield stress improves to 400 MPa
Dück et al. [46]	Cu–Ni power Infiltrated in Sn60PbAg at 200–432 °C, for 30–240 s	*SLS* Laser power: 160 W Layer thickness: 100 μm Scan spacing: 100 μm Scan speed: 400 mm/s	A model is developed to consider the capillary force and the pressure difference in the pore Capillary force and the pressure difference in the pore are two critical factors affect the infiltration performance Experiment shows that the infiltration depth reaches around 4–5 mm at a total wall thickness of 6 mm

Table 2 continued

Authors	Materials/preparation	Laser processing parameters	Effects/improvements/findings
Khaing and Lu, [47]	Mixture of nickel, bronze, and copper-phosphide Post-treatment: Epoxy infiltration at 60 °C, followed by oven treatment at 160 °C for 2 h	*DMLS* Layer thickness: 50 μm	Hardness increases from 26–33 to 65–69 HRB Roughness increases from 12–16 to 4–7 μm. Average density increases from 6.264 to 6.325 g/cm^3
Zhu et al. [48]	Copper and S–Cu–P mixture (volume ratio 60:40) Post-treatment: Infiltration with epoxy	*DMLS* Laser power: 120 W Scan spacing: 0.2 mm Scan speed: 200 mm/s Layer thickness: 75 μm	Hardness improves from 40 ± 7 to 66 ± 10 (HR 15T). Surface roughness Ra improves from 14–16 to 2–3 (μm). Relative density improves from 65 to 100%

conductivity. Thus, various types of iron-based alloys, as well as the associated MMCs, have been prepared successfully using additive manufacturing methods. Incorporation of ceramic particles is the most common way to strengthen iron-based alloys, and most studies show improved mechanical properties. However, the existing studies generally focus on static mechanical properties, including tensile, compression, and hardness. Fatigue properties of iron-based MMCs are much less studied, which continues to create challenges for the application of such MMCs in the real load-bearing scenarios.

Reinforced by TiC particles

TiC particle is the mostly adopted reinforcement in producing iron-based matrix composite. Higher microhardness and enhanced modulus of elasticity are observed when TiC is added into FeAl alloy during the SLM process [49]. The results show that TiC-reinforced FeAl intermetallic matrix composite bulk parts present a relatively smooth and dense melted microstructure, giving rise to the improved wear performance. Emamian et al. [50] study the temperature/microstructure relation in the laser cladding processed Fe–TiC MMC. It is found that low cooling rate could lead to a less uniform distribution of TiC particles in the matrix, while high cooling rate may become the source of micro-crack formation across the deposited layer. Later, such process is studied by a simulation approach [51], and the cooling rate and peak temperature during the process are predicted. The morphology of TiC particles and material microstructure can be tailored by controlling

cooling rate. Nano-TiC and nano-TiB$_2$ particles can be employed to reinforce 316L stainless steel during the SLM process, and improvements on hardness and anti-oxidation property are achieved [52]. A numerical analysis model is developed and verified by the nanoindentation results, which is able to optimize the controlling parameters in the SLM process. Gåård et al. [53] fabricate TiC particle-reinforced Fe–Ni alloy by DMLS. The dissolution of TiC promotes the FCC to BCC transition of the matrix phase. When the TiC addition is lowered to 30%, the bending strength, hardness, and wear performance of the composite are found inferior to conventionally manufactured hard metals. A few simulation studies have been performed to study the manufacturing process of TiC-reinforced iron MMCs. In the work of Amano et al. [54], a thermodynamics- and fluid dynamics-based numerical model is established to investigate how the processing parameters would affect the structure of nickel-coated TiC-reinforced 316L steel prepared by the LENS process. Besides, Alimardani et al. [55] develop numeric model to study the effect of temperature on the Fe–TiC composite by laser cladding process, and the simulation results help to optimize the processing parameters. With the addition of 9 vol% nano-TiC particles and followed by LSP at optimized parameters, the laser-sintered material shows a hardness increase of 61% as compared with the laser-sintered pure iron.

Reinforced by SiC particles

Ramesh et al. [56] reinforce the iron matrix by nickel-coated SiC particles using DMLS and characterize the

mechanical properties of the formed composites. The improvements in microhardness and abrasive wear resistance are observed in the composite material. A follow-up study [57] is performed to investigate the effect of SiC content and manufacturing parameters on the mechanical properties of a SiC/iron composite by DMLS. A negative correlation relation between the scan speed and hardness, and a positive correlation between the SiC content and coefficient of friction are observed. Similarly, Song et al. [9] employ the SLM process to synthesize Fe/SiC composite. It is discovered that the addition of SiC promotes the formation of martensite and pearlite in the matrix.

Reinforced by other ceramic materials

Other types of ceramic materials, such as TiN, WC, TiB$_2$, have also been used to reinforce steels fabricated by laser-assisted AM processes. For instance, the fatigue performance of DMLS-produced iron matrix composite reinforced by nano-TiN particles is investigated by Lin et al. [58]. The addition of TiN nanoparticles helps to increase the dislocation density during LSP (laser shock peening) and pin the dislocation propagation, thus improving residual stress stability. WC particles are found either partially or fully melted in the steel matrix during SLM, but a much higher wear resistance can be achieved [59]. Cold spray technique and SLM are combined to produce WC-reinforced MS300 steel, and improved wear resistance is observed [60]. TiB$_2$ particle is used to reinforce 316L stainless steel in the SLM process and the composite exhibits good combination of compression strength and ductility. It is found that the addition of 15 vol% reinforcement leads to a significantly lowered wear rate [61]. Moreover, calcium silicate (GaSiO$_3$) is used as reinforcement in SLM of 316L stainless steel [62]. The obtained composite is classified as ductile material, and the fracture surface shows both ductile and brittle characteristics. The addition of GaSiO$_3$ is found to improve corrosion resistance.

Reinforced by infiltration materials

Due to the large differences between iron and copper, as well as good bonding between them, copper is usually used as an infiltration material to make the AM-produced iron-based green parts fully dense. Dewidar et al. [63] investigate the processing parameters (e.g., laser power, scan spacing, and scan speed) on the mechanical properties (e.g., density, flexural strength, and flexural modulus) of high-speed steels by the SLS process. It is found that after infiltration with bronze, the flexural strength and modulus are significantly enhanced. In addition, Kumar and Kruth [64] investigate the infiltration of bronze particles into laser-sintered iron-based products and obtain a modest increase (around 5%) in the material density. Some studies also report using epoxy resin to infiltrate the iron green parts. In the work of Yan et al. [65], green parts are obtained by SLS of nylon-12 coated carbon steel powders and infiltrated by epoxy. Compared with the green parts, the infiltration yields improvements in material bending strength, tensile strength, and impact strength for more than 40 times, 7 times, and 2 times, respectively. In a similar fashion, Liu et al. [66] use the mixture of epoxy resin/iron powder as the starting material for SLS and infiltrate the green part by bronze after debinding process. It is observed that the pores are almost filled up in the infiltrated parts and significant increase in strength is also obtained.

Reinforced by carbon materials

There are a few studies on additive manufacturing of iron-based MMCs with carbon materials as reinforcements. The direct laser-sintered iron–graphite composite is found to consist of multiple phases, such as ferrite, martensite, carbide, and ledeburite [67]. Graphite plays an important role in densifying the final composite, because of the increased laser absorptance, the reduction of the melt pool surface tension, as well as the decrease in oxygen. A graphene oxide (GO)/iron MMC coating is fabricated using the SLS process [68]. The evaporation of solution agent promotes the vertical alignment of GOs in the matrix, as shown in Fig. 7. There is a coherent bonding between GOs and iron matrix, and the GOs are completely stretched due to directional vaporization of binder material. The application of such a GO/iron coating on stainless steel specimen improves the surface hardness and the fatigue performance (Table 3).
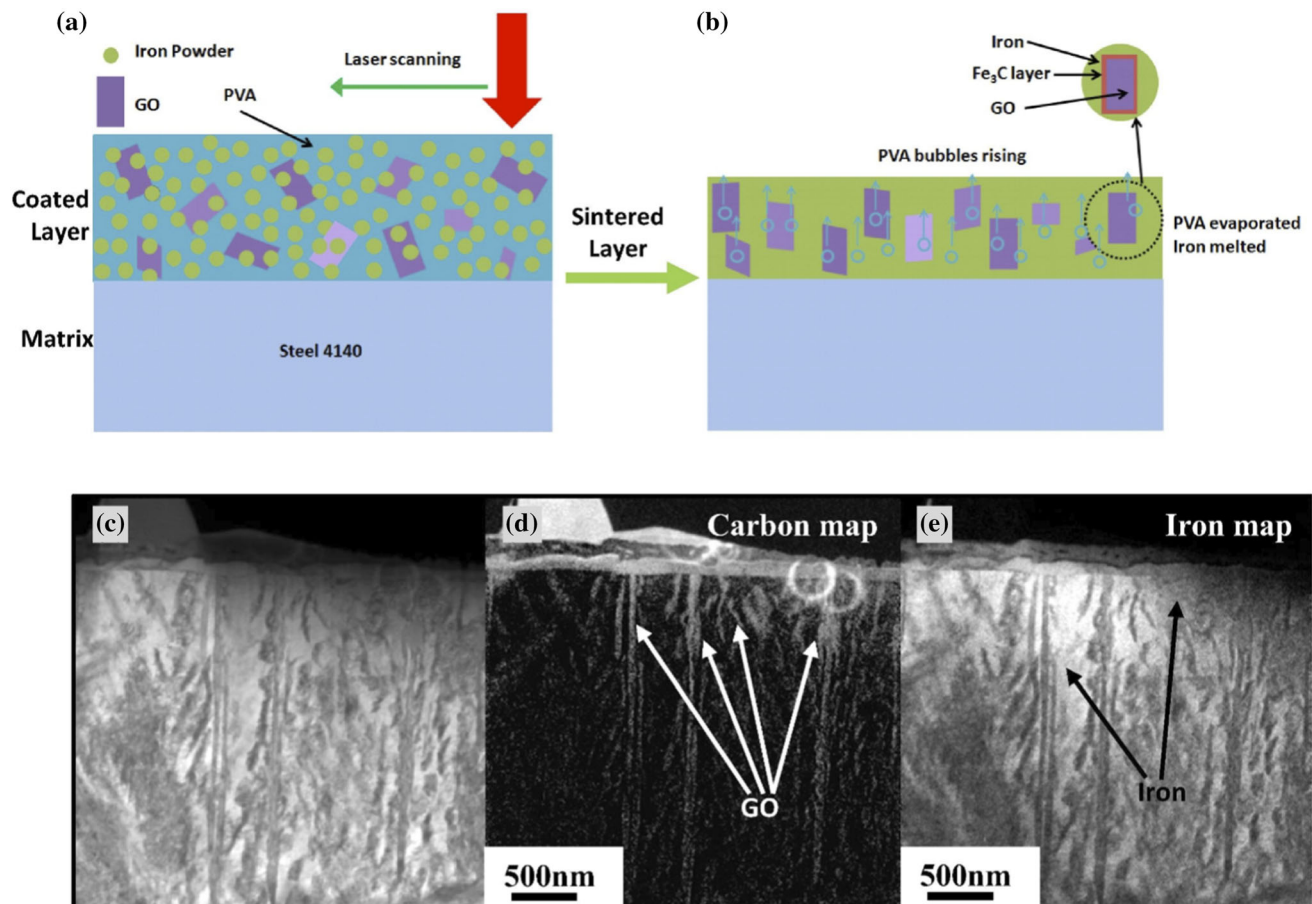
Figure 7 Laser deposition of GO–Fe nanocomposite layer, **a** schematic of coating process, **b** schematic of laser sintering process, **c** microstructure of as-built layer, **d** EDS mapping of carbon, and (e) EDS mapping of iron [68].

Nickel-based metal matrix composites

Nickel-based alloys have good high-temperature mechanical properties so that they are widely used for structural loading components in the high temperature environments of aerospace, energy, metallurgy industries. Additive manufacturing of Ni-based alloy has drawn much attention due to the decent laser absorption as well as the hard-to-machine nature of nickel-based alloys. Many studies have been carried out on fabricating nickel-based alloys through additive manufacturing methods. Due to similar physical properties between iron and nickel, reinforcement materials used in iron-based MMCs are generally suitable in nickel-based MMCs as well. Among them, TiC particle is probably the most adopted reinforcing material. The addition of ceramic particles during AM of nickel-based MMCs

has been reported to effectively enhance various mechanical properties, such as hardness, strength, and wear performance. However, the major gap of existing efforts lies in the insufficient investigation about high-temperature mechanical properties, given that nickel-based superalloy is widely used for high-temperature critical components. Therefore, the fundamental research about the reinforcement/matrix interaction of AM-built nickel-based MMCs during high-temperature service carries significant scientific merit.

Reinforced by TiC particles

The strengthening effects of three most deployed ceramic particles, namely SiC, Al_2O_3, and TiC, are compared in the LMD-produced Inconel 625 matrix composites [69]. The most outstanding mechanical

Table 3 Literature on Fe/Fe alloy matrix-based composites fabricated by laser-assisted additive manufacturing

Authors	Materials/preparation	Laser processing parameters	Effects/improvements/findings
Song et al. [9]	Fe (20 μm) and 2.2 wt% SiC (0.7 μm)	*SLM* Laser power: 100 W Spot size: 34 μm Scan speed: 330 mm/s Scan spacing: 40 μm Layer thickness: 50 μm	Addition of SiC leads to the disappearance of liquid front, due to the change in local instability and viscosity Addition of SiC leads to the formation of nano-sized iron grain and amorphous iron Much higher tensile strength is obtained after adding SiC, with a yield strength of 302 MPa and an ultimate strength of 764 MPa, compared with the ultimate strength of 357 MPa of as-fabricated iron
Song et al. [49]	FeAl (Fe–35Al wt%) and TiC powder, mass ratio 70:30	*SLM* Laser power: 90 W Spot size: 34 μm Scan speed: 200 mm/s Layer thickness: 50 μm	The microhardness is improved from 780 to 830 MPa Modulus of elasticity is improved from 21 to 70 GPa Wear rate is improved from 4.8×10^{-7} to 7.5×10^{-9} mm^3 m^{-1} N^{-1}.
Emamian et al. [50]	Fe, Ti, and C at weight ratio of 70:24.9:5.1	*LMD* Maximum laser power: 1100 W	In situ TiC particles are formed Experiment and simulation indicates that the distribution of the TiC particles within the deposited tracks varies with the local temporal cooling rate Higher cooling rate results in more uniform distribution of TiC particles
Emamian et al. [51]	Fe, Ti, and C at weight ratio of 70:24.9:5.1	*LMD* Laser power: 480–980 W Scan speed: 1.75–3.1 mm/s Feed rate: 2–4 g/min	Final microstructure strongly depends on cooling rate powder's chemical composition Morphology of carbide is related to cooling rate
Biedunkiewicz et al. [52]	316 stainless steel, 5–50 vol% powders containing TiC (40–100 nm) and TiB$_2$ (60–120 nm)	*SLM* Laser power: 100 W Layer thickness: 50–75 μm	Dispersion of nanocrystalline particles in steel matrix is overall unifrom By adding 50 vol% nc-TiC, the microhardness is increased by 300% By adding 20 vol% nc-TiB$_2$, the microhardness is increased by 400%
Gåård et al. [53]	Fe–Ni alloy (7 μm) and 30–80 wt% TiC (< 1 μm)	*DMLS* Parameters not available	Dissolution of TiC promotes the FCC to BCC transformation of matrix The average coefficient of thermal expansion is increased, leading to cracking of composite Mechanical performance is limited due to porosity
Amano et al. [54]	Stainless steel 316L (45–105 μm) and 15 wt% nickel-coated TiC (1–45 μm)	*LENS* Laser power: 650 W	The proposed model shows good agreement with experiments in calculating cooling rate The equilibrium solidification phase transformation for 316L stainless steel is primary ferrite solidification
Alimardani et al. [55]	Fe, Ti, and C at weight ratio 70:24.9:5.1	*LMD* Laser power: 885 W Scan speed: 2 mm/s Powder feed rate: 4 g/min	Simulation indicates that the temperature gradient decreases along with the deposition process, due to the increase in substrate temperature The increase in melt pool temperature and decrease in cooling rate changes the distribution of TiC particles

Table 3 continued

Authors	Materials/preparation	Laser processing parameters	Effects/improvements/findings
Ramesh et al. [56]	Iron and 1–3 wt% nickel-coated SiC particles	*DMLS* Laser power: 180 W Spot size: 0.4 mm Scan speed: 100 mm/s Scan spacing: 20 mm Layer thickness: 50 μm	Increase in microhardness and decrease in density are observed with the increase in SiC content Microhardness is improved from 240 to 400 VHN Formed composite exhibits excellent wear resistance (improved by 300%)
Ramesh & Srinivas, [57]	Iron and 5 wt% nickel-coated SiC particles	*DMLS* Laser power: 180 W Spot size: 0.4 mm Scan speed: 50–125 mm/s Scan spacing: 20 μm Layer thickness: 50 μm	Lower sintering speed leads to higher density, higher hardness, and higher wear resistance Addition of SiC particles results in increased COF
Lin et al. [58]	Iron (4 μm) and TiN (20 nm)	*SLS* Parameters not available	Post-laser shot peening significantly improves fatigue performance The existence of nanoparticles increases the dislocation density and pins the dislocation movement
Kang et al. [59]	WC particles (4 μm) and maraging steel (41 μm), weight ratio 15:85	*SLS* Laser power: 275 W Scan speed: 1360 mm/s Layer thickness: 50 μm	Wear rate decreases from 6.2×10^{-5} to 0.8×10^{-5} mm^3/(N*m) after adding WC
Yan et al. [60]	WC particles (1–6 μm) and MS300 steel powder (33–40 μm), weight ratio 15:85	Cold spray and SLM *Cold spray* Pressure: 3 MPs Gas temperature: 500 °C Travers speed: 100 mm/s *SLM* Laser power: 285 W Layer thickness: 50 μm Hatch distance: 50 μm Scan speed: 960 mm/s	The material obtained by cold spray shows a slightly higher microhardness than that obtained by SLM, mainly due to severe work hardening introduced in cold spray Different evolution features of WC are found in the two difference AM processes Agglomeration of WC particles results in fluctuation of friction rate during wear tests
AlMangour et al. [61]	2.5–15 vol% TiB$_2$ particles (2–12 μm) and 316L steel powder (45 μm)	*SLM* Laser power: 100 W Spot size: 0.18 mm Scan spacing: 0.12 mm Scan speed: 83.3 mm/s Layer thickness: 50 μm	Good combination of compressive strength and ductility is obtained The homogeneously dispersed TiB$_2$ particles form a cellular nanostructured array with thickness of about 170 nm Increase in reinforcement content from 2.5 to 15 vol% leads to the formation of pores but significantly improves wear resistance
Zheng et al. [62]	0–15 wt% CaSiO$_3$ powder (5 μm) and 316L steel powder (35 μm)	*SLM* Laser power: 140 W Spot size: 0.15 mm Scan spacing: 70 μm Scan speed: 350 mm/s Layer thickness: 20 μm	Relative density can be kept with lower than 5 wt% reinforcement Corrosion resistance is enhanced, meaning that the obtained composite can be used as biomaterials As the reinforcement content increases beyond 5 wt%, the mechanical properties of composite quickly deteriorate

Table 3 continued

Authors	Materials/preparation	Laser processing parameters	Effects/improvements/findings
Dewidar et al. [63]	High-speed steel Post-treatment: Infiltrated with bronze at 1060 °C for 3 h	*SLS* Laser power: 50 W Scan speed: 1 mm/s Scan spacing: 682 µm Layer thickness: 500 µm	Flexural strength increases from 250 to 631 MPa Flexural modulus increases from 79 to 123.7 GPa
Kumar and Kruth [64]	Mixture of 15% Cu, 20% Ni, 50% Fe, and 15% Fe_3P Post-treatment: Infiltration with bronze at 1050 °C for 5 h (total 25 h including temperature ramp-up process)	*SLS* Laser power: 60 W Scan speed: 60 mm/s Scan spacing: 100 µm Layer thickness: 100 µm Spot size: 600 µm	Brinell hardness increases from 85 to 177 Surface roughness improves from 7.4 to 8.8 µm Bending strength increases from 316 to 576 MPa Density increases from 6.3 to 7.5 g/cm^3
Yan et al. [65]	Carbon steel with nylon-12 binder Post-treatment: Binder removal in furnace then infiltrated in epoxy resin at 100 °C for 10 min	*SLS* Laser power: 12 W Scan speed: 2000 mm/s Scan spacing: 100 µm Layer thickness: 100 µm	Bending strength improves from 1.87 to 93.4 MPa Bending modulus improves from 0.79 to 14.7 GPa Tensile strength improves from 9.34 (binder free) to 70.3 MPa Impact strength improves from 5.56 to 12.4 kJ/m^2
Liu et al. [66]	Iron with 5 wt% singular epoxy Post-treatment: Sintering at 1150 °C for 1 h, then infiltrated in bronze powder at 1100 °C	*SLS* Laser power: 15 W Scan speed: 2000 mm/s Scan spacing: 100 µm Layer thickness: 100 µm	Tensile strength reaches 230 MPa Final density is almost 100% theoretical density Pores are almost filled bronze
Simchi and Pohl [67]	Iron (68 µm) and graphite (2 µm)	*DMLS* Laser power: 70–225 W Scan speed: 50–600 mm/s Scan spacing: 0.1–0.3 mm Layer thickness: 0.1 mm	Addition of graphite enhances the densification of iron powder and improves surface quality Addition of graphite changes the internal pore structure of sintered parts Dissolved carbon changes the surface tension and viscosity of iron melt, thus increasing the sintering kinetics
Lin et al. [68]	Iron (4 µm) and 2 wt% single layer graphene oxide (thickness 0.7–1.2 nm)	*SLS* Laser power: 100 W	Bonding between graphene and iron matrix is coherent The distribution of graphene oxide is uniform Surface hardness is improved by 20% Fatigue limit is improved by 50%

properties (high hardness at uncompromised material ductility and integrity) are brought by the addition of TiC particles. The addition of TiC particles is also reported to benefit the anti-oxidation performance [70] and to help refine the grain size in LMD-processed Inconel 625 [71]. Several works investigate the parameter optimization of TiC-reinforced Inconel 718 [72] [73]. It is found that the increase in laser power density results in a smoothed structure of reinforcement particle, but excessive laser power density may cause the coarsening of reinforcement and thus lead to weak interfacial layer. Nearly fully dense Inconel 718/TiC composite is obtained under optimized processing parameters in the SLM process [74]. TiC particles have also been used for the development of functionally gradient metal matrix composites (FGMMC) by LMD process [75]. The TiC particles exhibit a uniform and gradual distribution in the FGMMC, as shown in Fig. 8. Over 30 vol% of TiC leads to a columnar to equiaxed transition and enhanced wear performance. Moreover, Cui et al. [76] fabricate the Ni–Ti–C composite coating on cast
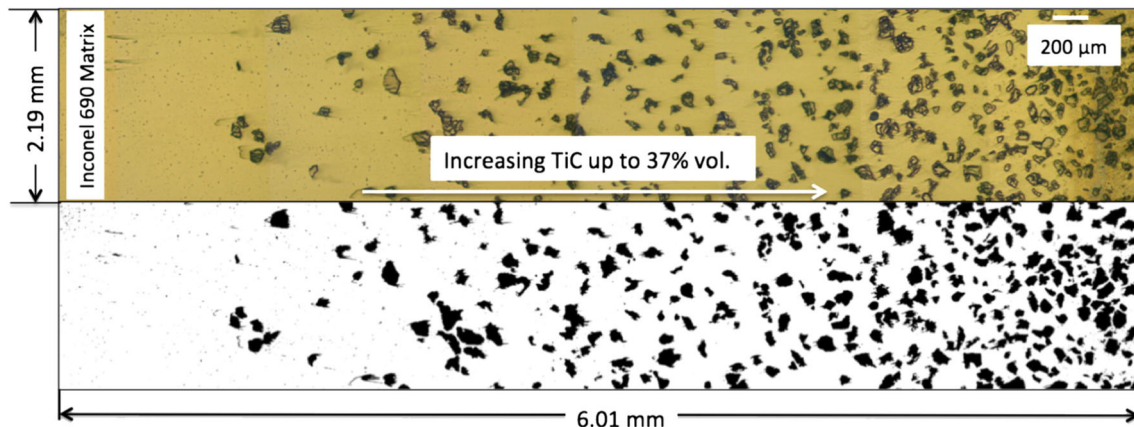
Figure 8 Micrograph of a TiC/In690 functional gradient material [75].

iron substrate using laser cladding technique. The starting material is a mixture of nickel, titanium and graphite, and the in situ formation of TiC is characterized. The formation mechanism of TiC is determined as nucleation growth. The hardness and wear performance of the TiC-reinforced coating are significantly enhanced. Zheng et al. [77] test both uncoated and Ni-coated TiC particles to fabricated Inconel 625 composite using the LENS technology. The results indicate that Ni coating of TiC can effectively improve the manufacture process in terms of flowability of melt pool, the integrity of interface, and interaction between laser and TiC particles. Also, a higher density of dislocation is observed around reinforcing particles due to the large difference of CTE (coefficient of thermal expansion) between TiC and matrix. Wang et al. [78] perform heat treatment on nano-TiC-reinforced Inconel 718 made by SLM, and results show that nano-TiC particles play an important role in strengthening the material by suppressing microstructure coarsening during post-solution treatment.

Reinforced by other materials

Other than TiC, the use of reinforcement including WC, TiB$_2$, and graphene to strengthen nickel-based alloy has also been reported. For instance, wear performance is usually the focus when WC particles are used as reinforcement. In the study of Rong et al. [79], a very low and stable COF (about 0.35) and wear rate (2.5×10^{-4} mm^{-3} N^{-1} M^{-1}) are achieved by adding 25 wt% WC particles into Inconel 718. The gradient interface between WC particles and matrix plays an important role in improving the wear performance by hindering the propagation of cracks, as shown in Fig. 9. Similar WC particle-reinforced Inconel 718 is reported by Nguyen et al. [80]. It is found that WC particles have a hindering effect on the columnar growth of matrix grains and thus refine the microstructure. Moreover, a drop of strength will happen if the amount of WC reaches 15 wt%. TiB$_2$ is used to reinforce Inconel 625 superalloy, and an in situ interfacial layer rich in Mo and Ti is formed between the reinforcement particle and matrix, which is believed to prevent crack formation [81]. Up to 1 wt% graphene nanoplatelets are added into Inconel 718 superalloy by using the SLM process [82, 83]. There is a significant improvement of strength and Young's modulus but accompanied by a considerable drop in material ductility. Meanwhile, the wear performance significantly improves thanks to a self-lubricating effect of graphene nanoplatelets. Graphene nanoplatelets are found to suppress the microstructure from coarsening during post-solution treatment of graphene/Inconel 718 composite [84] (Table 4).

Titanium-based metal matrix composites

Titanium-based materials have wide advantages such as high strength-to-weight ratio, good high-temperature performance, and good biocompatibility. Therefore, they have been widely used in aerospace, biomedical, and automotive industries. Laser-assisted additive manufacturing of Ti-based MMCs has
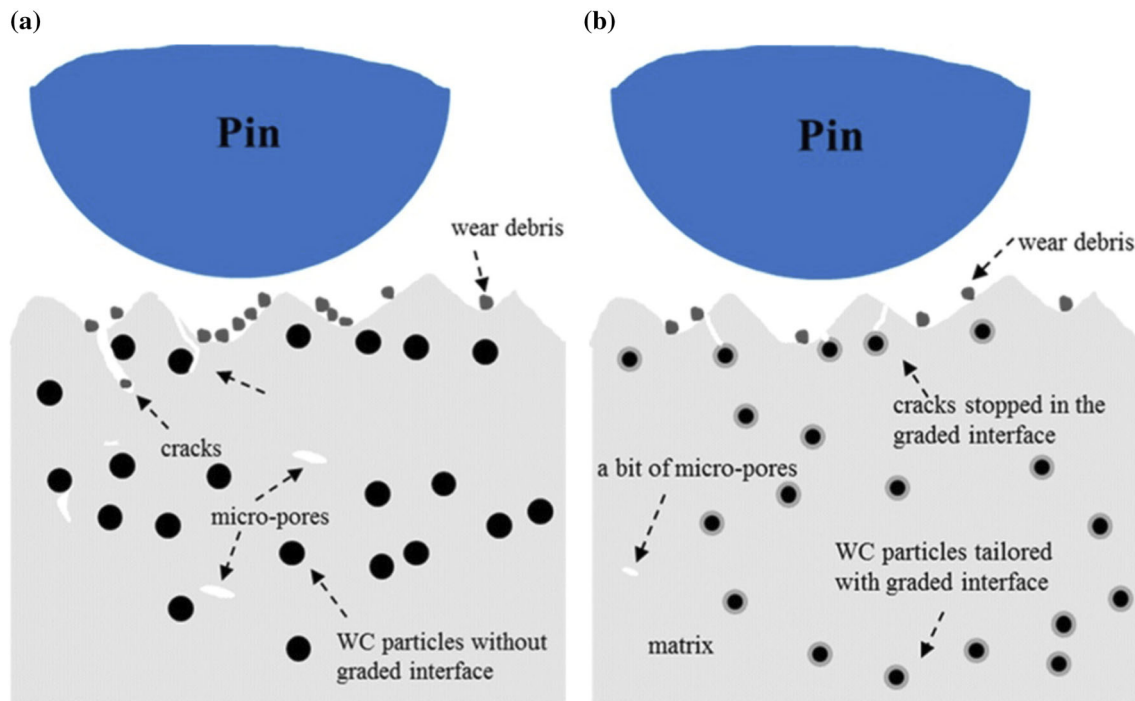
(a)   **(b)**

Figure 9 Schematics showing how graded interface improves the wear performance **a** without a graded interface, **b** with graded interface [79].

been extensively investigated in recent years. The strengthening effects of various types of reinforcement have been evaluated for the titanium-based MMC system, and TiC is again among the most adopted reinforcements. Unlike other metals, the choice of reinforcement materials for titanium-based MMCs is relatively limited, mainly due to the reactive nature of titanium. Titanium matrix can react with many external phases under high temperature and oxidation is highly likely to occur, promoting the formation of various carbide, oxide, and intermetallic phases, which are detrimental to the overall properties [85]. Thus, the trial-and-error cost of synthesizing titanium-based MMCs is high. Due to this reason, the use of thermo-dynamic calculation theories, such as calculation of phase diagram, is believed to expedite the design of titanium-based MMCs through AM.

Reinforced by TiC particles

TiC is extensively adopted as the reinforcing material in the processing of Ti alloy matrix composites via laser-assisted AM processes. Gu et al. [86] use mechanically milled Ti–Al–graphite powder mixture as the starting material to obtain TiC-reinforced

Ti(Al) matrix composite through the SLM process. The major matrix phase of SLM-produced composite is $TiAl_3$ and the minor phase is Ti_3Al_2, while TiC is in situ formed as the reinforcing phase. To obtain the in situ formed TiB and TiC, Zhang et al. [87] adopt laser deposition to process the powder mixture of Ti6Al4V titanium alloy and B_4C. Microstructure observations show that the formed TiB appears to be needle like and prismatic, while TiC tends to be granular. However, the tensile property of the composite is limited due to the existence of some unreacted B_4C. Gu et al. [88] focus on similar in situ formation process of TiC during the laser deposition, where Ti and SiC are used as starting material to form TiC-reinforced Ti_5Si_3 matrix composite. Laser energy density is varied to see its effect on product quality. Ni-coated TiC powder is directly mixed with Ti6Al4V powder, and the blended powder mixture is used as the starting material for the LMD process [89]. Melting and re-solidification of TiC particles in the matrix are observed during the LMD process. This results in fine microstructure and strong interface bonding between TiC particles and matrix, as well as improved tensile strength. Mahamood et al. [90] adopt the same process of manufacturing

Table 4 Literature on Ni/Ni alloy matrix-based composites fabricated by laser-assisted additive manufacturing

Authors	Materials/preparation	Laser processing parameters	Effects/improvements/findings
Cooper et al. [69]	Inconel 625 (31.28 μm) and 5 wt% TiC (0.44 μm)	*SLM* Laser power: 800–1000 W Layer thickness: 100 μm Scan speed: 6–7 m/s Scan spacing: 0.5 μm	Addition of TiC results in 30% increase in hardness Partial dissolution of TiC is observed, which leads to the rounding of particles compared to their original angular morphology
Hong et al. [70]	Inconel 625 (15–45 μm) and 5 wt% TiC (4–7 μm)	*LMD* Laser power: 600 W Layer thickness: 250–300 μm Scan speed: 500 min/min Powder feed rate: 2.4 g/min	Incorporation of TiC results in grain refinement The addition of TiC enhances high-temperature oxidation resistance, and the mass gain after 100 h oxidation at 800 °C decreases from 1.414 to 0.323 mg/cm^2 The oxidation surface mainly consists of Cr_2O_3 for pure Inconel 625, while for TiC/Inconel 625 composites, it consists of Cr_2O_3 and TiO_2
Bi et al. [71]	Inconel 625 (20–45 μm) and 0.25–1 wt% TiC (80–150 nm)	*LMD* Not mentioned	Adding 1 wt% TiC improves the hardness to 321.9 HV, compared to unreinforced pure Inconel 625 (285.8 HV) Ultimate tensile strength is increased from 840 to 996 MPa Nano-TiC functions as grain refiner to obtain a refined microstructure
Hong et al. [72]	Inconel 718 (15–45 μm) and 20–30 wt% TiC (22.5–45 μm)	*LMD* Laser power: 0.7–1.3 kW Scan speed: 500 min/min Powder feed rate: 2.4 g/min	For laser energy input per unit length 80–120 kJ/m, coherent interfacial (Ti, M)C (M = Nb and Mo) layer is formed As the laser energy input per unit length increases from 80 to 160 kJ/m, the microhardness is increased from 375 to 450 HV$_{0.2}$, and the wear rate is decreased from 4 to 0.5 × 10^{-13} m^3 N^{-1} m^{-1}
Gu et al. [73]	Inconel 718 (15–45 μm) and TiC (22.5–45 μm)	*LMD* Laser energy density: 280–490 J × mm^{-3} Scan speed: 500 min/min Powder feed rate: 2.4 g/min	TiC$_x$ reinforcing particles change from irregular to smoothened morphology Microstructure is refined as laser energy density increases. Optimized laser energy density is determined as 420 J × mm^{-3} to achieve a low coefficient of friction of 0.38 and wear rate of 1.8 × 10^{-4} mm^3 N^{-1} m^{-1}
Jia et al. [74]	Inconel 718 (15–45 μm) and 10 wt% TiC (50 nm)	*SLM* Laser power: 80–130 W Scan speed: 400 mm/min	Relative density increases as laser energy density increases Wear resistance decreases from 5.4 to 2.6 × 10^{-4} mm^3 N^{-1} m^{-1} as laser energy density increases from 3 to 5 kJ/mm^3
Wilson and Shin [75]	Inconel 690 (44–149 μm) and 0–49 vol% TiC (similar particle size)	*LMD* Laser power: 350 W Layer thickness: 250–300 μm Scan speed: 17 mm/s Scan spacing: 0.38–0.45 mm	For TiC particles over 30 vol, refinement of matrix microstructure is seen Hardness values of pure Inconel 690 and reinforced Inconel 690 are 15 and 40 HRC The composite exhibits enhanced wear resistance, and the volume loss is reduced from 3.8 to 1.9 mm^3 (5 lbs load and 200 m sliding distance)
Cui et al. [76]	Mixture of Ni, Ti, Graphite	Laser cladding	TiC with various shapes and sizes are in situ formed After being coated with the TiC-reinforced Ni, the hardness and wear resistance of substrate are significantly enhanced

Table 4 continued

Authors	Materials/preparation	Laser processing parameters	Effects/improvements/findings
Zheng et al. [77]	Inconel 625 (45–125 μm) and 20 wt% Ni-coated TiC	*LMD* Laser power: 280 W Scan speed: 14.8 mm/s	Coating Ni on TiC particles significantly increases the flowability of the mixed powders and improves the integrity of the TiC/matrix interface With 20 wt% Ni-coated TiC, material yield strength is increased from 550 to 660 MPa, compared to unreinforced LMD-produced Inconel 625
Wang et al. [78]	Inconel 718 (15–55 μm) and 0.5 wt% nano-TiC particles (mean size 50 nm)	*SLM* Laser power: 200 W Layer thickness: 30 μm Scan spacing: 60 μm Scan speed: 7 m/s	Nano-TiC has significant strengthening effect in both as-built and heat-treated conditions The composite undergoes recrystallization during heat treatment Nano-TiC particles suppress the microstructure from coarsening during heat treatment The maximum tensile strength of 1370 MPa is obtained under 980 °C + aging condition, showing a 16% increase as compared to the unreinforced Inconel 718
Rong et al. [79]	25 wt% WC particles (25–45 μm) and Inconel 718 (15–45 μm)	*SLM* Laser power: 110 W Spot diameter: 70 μm Scan spacing: 50 μm Scan speed: 350–650 mm/s	The mean microhardness reaches 392 $HV_{0.1}$ Very low COF (about 0.35) and wear rate (2.5×10^{-4} mm^{-3} N^{-1} M^{-1}) The graded interface between WC and matrix prevents the formation of cracks at the interface
Nguyen et al. [80]	5–15 wt% WC particles in Inconel 718 particles (both powders range 13–53 μm)	*SLM* Laser power: 180 W Spot diameter: 130 μm Scan spacing: 150 μm Layer thickness: 25 μm Scan speed: 850 mm/s	WC particles have a hindering effect on the columnar growth of matrix grains and thus refine the microstructure Drop of strength is observed if the amount of WC reaches 15 wt% UTS is increased by 20% at filler content of 10 wt%
Zhang et al. [81]	5 wt% TiB_2 (5–12 μm) and Inconel 625 (14–45 μm)	*SLM* Laser power: 80–120 W Scan spacing: 100 μm Layer thickness: 50 μm Scan speed: 100–300 mm/s	Ti and Mo-rich interface is formed between the TiB_2 particle and matrix Young's modulus increases by 23% and hardness increases by over 100%, under a laser energy density of 1200 J/m
Wang et al. [82]	0.25–1.0 wt% graphene nanoplatelets (5–50 μm) and Inconel 718 powder (40 μm)	*SLM* Laser power: 200 W Layer thickness: 30 μm Scan speed: 7 m/s	UTS is increased by over 50%; however, there is a considerable drop in ductility Young's modulus is increased by about 40%
Xiao et al. [83]	1.0 wt% graphene nanoplatelets (5–50 μm) and Inconel 718 powder (40 μm)	*SLM* Laser power: 200 W Layer thickness: 30 μm Scan speed: 7 m/s	An in situ protective layer on sample surface is formed during the wear test The friction of coefficient during wear test is reduced by 66%

Ti6Al4V/TiC composite material. Laser scanning velocity is varied to study its effect on microstructure and mechanical behavior of the composite, and the optimal scanning speed is obtained. A similar work on studying the effect of laser scanning speed can be seen in Gu et al.'s study [91], in which TiC reinforcement particles are mixed with Ti particles for the SLM process. TiC particles are added in Ti to make composite coating by LMD process [92], and the wear performance of the TiC-reinforced composite coating is investigated. It is found that microhardness can be significantly improved by adding 40 vol% TiC particles, a 15-fold wear rate reduction is observed as well. Besides that micro-sized TiC particles are extensively adopted as reinforcement in laser-assisted AM, the use of nano-sized TiC particles is also addressed in the literature [93]. As shown in Fig. 10, the wear test indicates that the adhesive wear mechanism is dominant when filler content is below 17.5 wt%. As

the content of nano-TiC exceeds this amount, the TiC particles lose nanostructure and become coarsened, leading to a decrease in wear performance.

High-temperature creep performance of 10.8 vol% TiC particulates-reinforced TA15 alloy fabricated by LMD is investigated at 873 K and 923 K by Liu et al. [94]. The microstructure of as-deposited MMC mainly exhibits near-equiaxed and coarsened dendritic morphology. It is shown that the TiC-reinforced composite exhibits superior creep resistance compared to the monolithic titanium alloy. TiC particles play an important role in increasing the creep rupture performance due to the load transfer from the matrix and refinement of the Widmanstätten matrix. The laser-deposited TiC/TA15 composite possesses superior creep performance as compared to a similar composite fabricated by the traditional method, as shown in Fig. 11. In the work of Zhang et al. [95], functional gradient Ti-matrix composite with
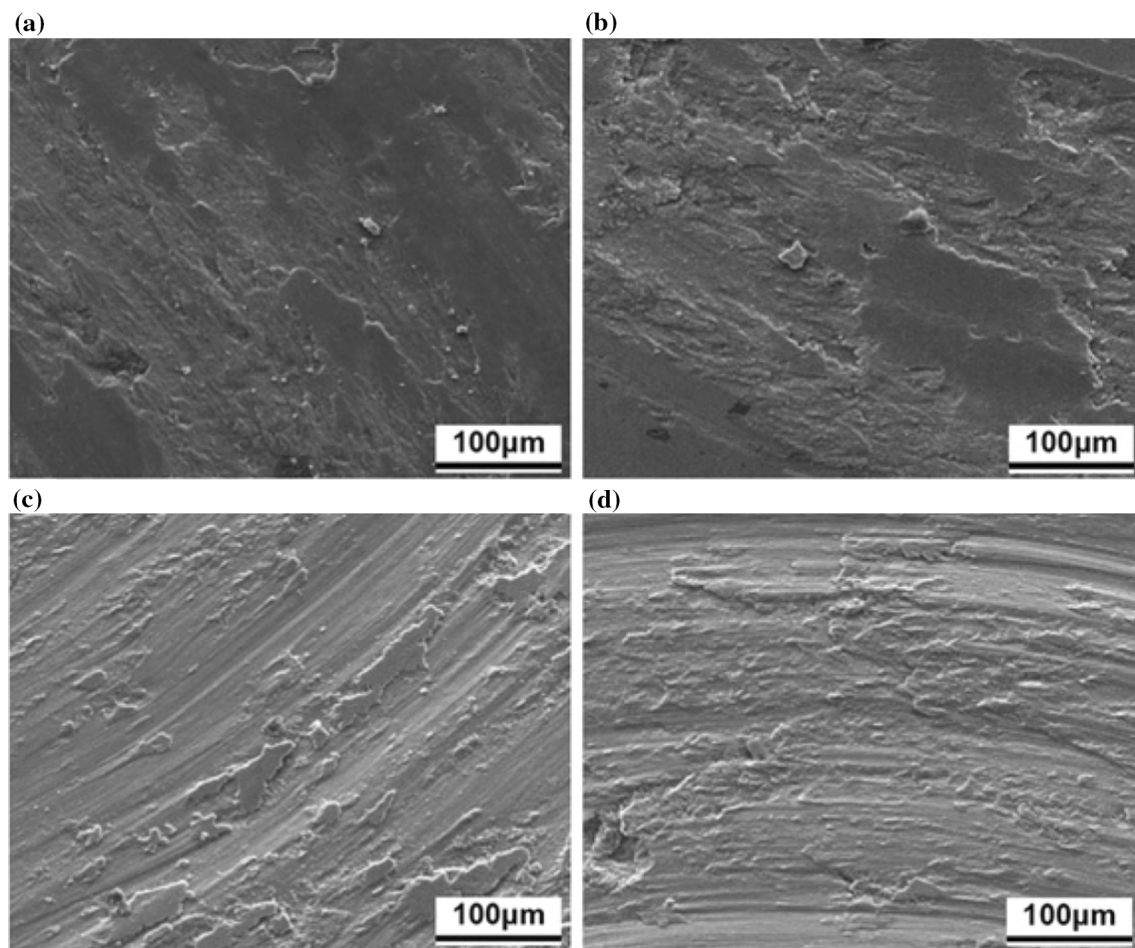

Figure 10 Morphologies of worn surfaces of nano-TiC-reinforced Ti MMCs at various content of reinforcement, **a** 7.5 wt%, **b** 12.5 wt%, **c** 17.5 wt%, and **d** 22.5 wt%. [93].
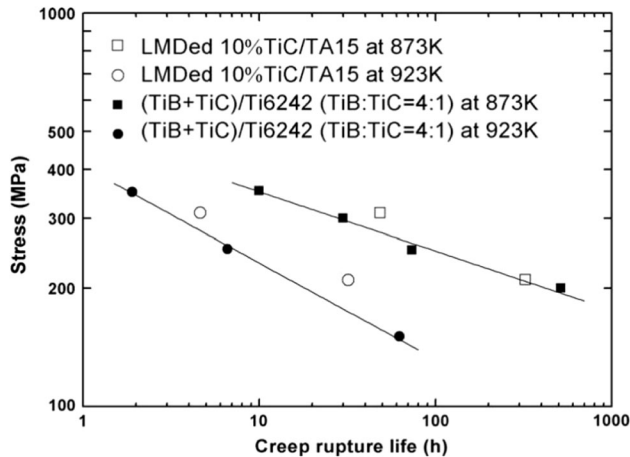
Figure 11 Laser-deposited TiC/TA15 composite show superior creep performance as compared to similar composites fabricated by traditional methods [94].

0–40 vol% TiC reinforcement is laser-deposited by varying the powder feed rate. It is found that the increase in TiC addition leads to the increase in the hardness and tensile strength of composite material but a decrease in the ductility. Meanwhile, the partially melt and solidified TiC particles act as the microstructure refiner. Based on the similar concept of functional gradient composite material, Ti6Al4V and Ti6Al4V/TiC dual material transition joints are manufactured using the LMD method [96]. Different designs of material transitions, such as butt joint, gradient joint, and interlocking joint, are fabricated by controlling the ratio of TiC to Ti6Al4V during the deposition process. The results indicate that the interlock design yields best tensile performance and

all the joints survived in the three-point loading test. Shishkovsky et al. [97] produce the Ti–TiB$_2$ gradient composite material and show that the microhardness increases as the content of TiB$_2$ increases. The XRD spectrum suggests that although some peaks of TiB$_2$ still exist, most TiB$_2$ particles disappear after laser treatment, as shown in Fig. 12.

Reinforced by other materials

In the literature, it is reported that Ti or Ti-based alloys are also reinforced by particles other than TiC in laser-assisted AM processes. TiB-reinforced Ti matrix composites are synthesized through SLM process of Ti–TiB$_2$ powder mixture [98, 99]. TiB is formed through the reaction between Ti and TiB$_2$, and the in situ formed TiB appears to be needle shaped, and the microstructure of Ti matrix is significantly refined. The composites show superior mechanical properties compared with the material obtained by the powder metallurgy process. Farayibi et al. [100] investigate the corrosion resistance of WC-reinforced Ti6Al4V alloy fabricated by laser cladding. Thanks to the uniformly distributed reaction products such as nanoscale TiC and W, the composite with 76 wt% WC particles exhibits up to 13 times better erosion resistance compared with wrought Ti6Al4V, as shown in Fig. 13 (Table 5).
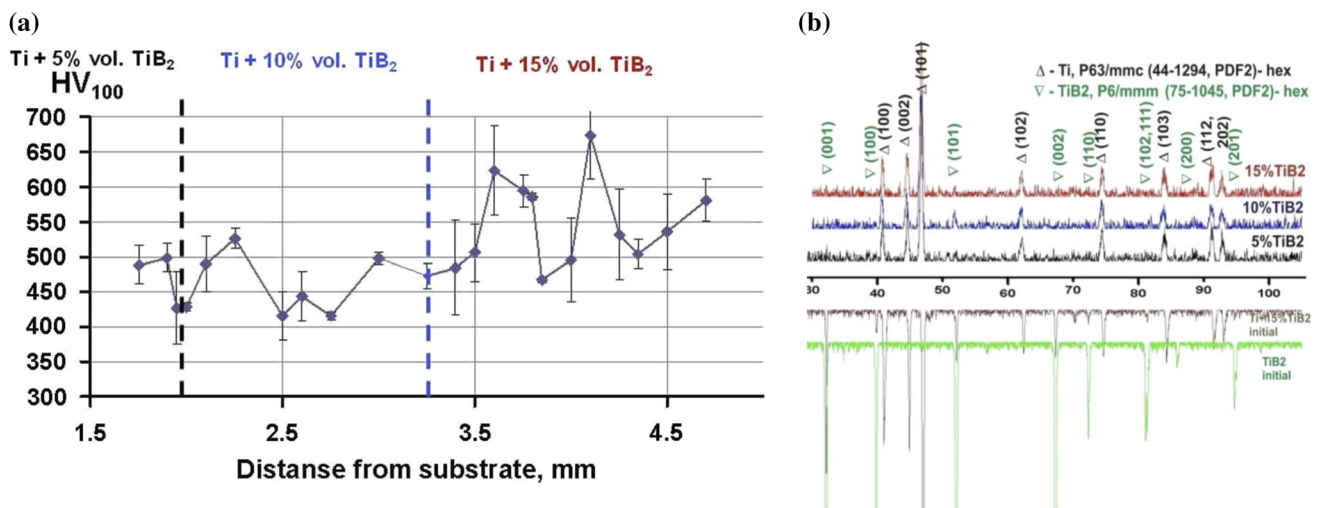

Figure 12 Microhardness and phase constituents of a Ti–TiB$_2$ functional gradient composite material produced by SLM [97].
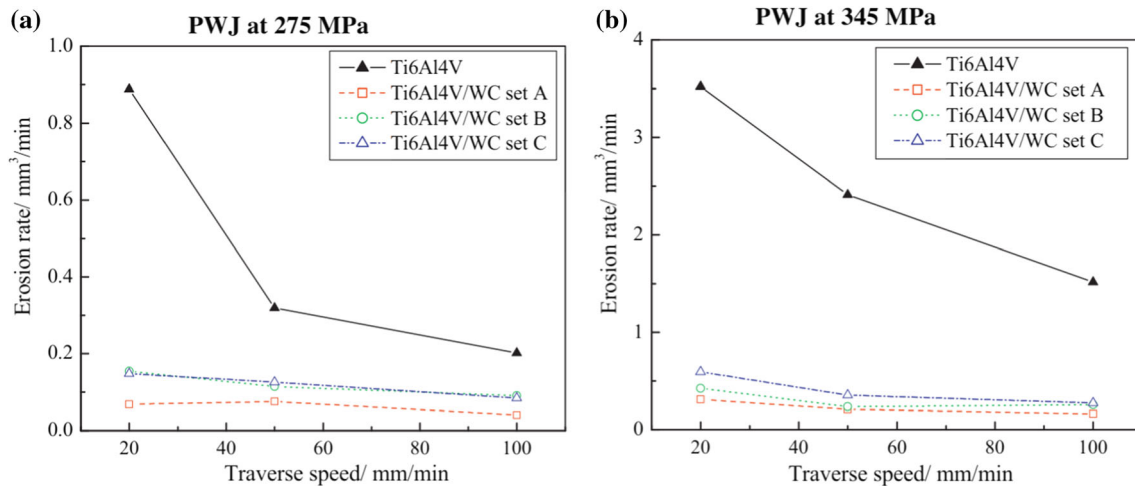
Figure 13 Comparison of erosion rate between WC reinforced and Ti6Al4V and pure Ti6Al4V obtained under plain water jet (PWJ) pressure of **a** 275 MPa, **b** 345 MPa [100].

Other metal matrix composites

Beside those frequently used metals/alloys as mentioned in previous sections, there are also a few AM studies that use other metals and alloys as the matrix materials. For example, Sun et al. [101] prepare a ZrB_2-reinforced Zr matrix composite by SLS. The starting powders consist of ZrB_2 and 30–50 wt% Zr. The sintered material exhibits good density and hardness value. Meanwhile, TiC-reinforced Zr matrix composite manufactured by LMD is presented by Ochonogor et al. [102]; Zr powders are mixed with 10–30 wt% TiC powders. It is found that the Zr metal reacts with the TiC to form ZrC, leaving Ti in solid solution. A few studies focus on Mg-based MMCs for better electrical performance. For instance, in the study of Zhang [103], $LaNi_5$–Mg_2Ni composite, an electrode material with high hydrogen storage capability, is fabricated by SLM. With the weight percentage of Mg_2Ni varying from 10 to 30%, several phases are detected in the sintered material (i.e., $LaNi_5$, $LaNi_4Mg$, and $LaMg_2Ni_9$), but with significant variation in amount. This leads to different electrochemical performances, in terms of discharge capabilities and the number of cycles for activation. In addition, Mg–20 wt% $LaNi_5$ composite is obtained by using the same method [104]. Phases identified within the material are Mg, Mg_2Ni, and $LaMg_{12}$. It is also indicated that Mg particles are surrounded by the network consisting of eutectic Mg + Mg_2Ni layers and small $LaMg_{12}$ blocks, which favors the improvement of activation property of electrodes.

Challenges and Research Opportunities

General challenges in metal AM

Additive manufacturing is a technology that has been enthusiastically pursued in recent years. Despite the advantages of metal additive manufacturing, there exist challenges that need to be addressed before the potential of AM can be fully explored. Those challenges occur at different levels, starting with the initial design to the final manufacturing stage, including a wide array of issues such as raw material qualification, process control, quality assurance, and industry standards. For instance, residual stress is a major obstacle in achieving consistent geometry in laser-assisted AM processes. It is usually generated due to the high thermal gradients formed in rapid heating and cooling cycles. The temperature differences in the irradiated region produce transient thermal strains at the different surface and depth locations, and such strain is retained after heat is removed [105, 106]. Solid-phase transformation during the complex thermal history is also reported to induce significant residual stress [107]. Another major challenge of laser-assisted AM lies in the fact that only limited materials have appropriate interaction with high energy beam. For example, AM of pure copper has tremendous challenges due to copper's high thermal conductivity. The melting area experiences rapid heat dissipation and high local thermal gradients, resulting in delamination, layer curling, and part failure. For aluminum alloys, the

Table 5 Literature on Ti/Ti alloy matrix-based composites fabricated by laser-assisted additive manufacturing

Authors	Materials/preparation	Laser processing parameters	Effects/Improvements/findings
Gu et al. [86]	Ti, Al, and C at weight ratio of 2:1:1	*SLM* Laser power: 800 W Scan speed: 100 mm/s Scan spacing: 160 μm Layer thickness: 150 μm Spot size: 300 μm	Increasing milling time of powder mixture changes the morphology from irregular shape to fine equiaxed shape In situ nano-Ti(Al) and TiC particles are formed, the major phase is identified as $TiAl_3$, and the product exhibits refined microstructure
Zhang et al. [87]	TC4 and 5 wt % B_4C powder mixture	*LMD* Laser power: 1.8 kW Scan speed: 4 mm/s Powder feed rate: 2.65 g/min for TC4 and 0.14 g/min for B_4C	In situ reaction occurs during the LMD process TiB and TiC with fraction of 25% are formed A thin skull of reaction product formed around the unreacted B_4C weakens the interface bonding, resulting in reduced properties
Gu et al. [88]	Ti (45 μm) and SiC (13 μm) at weight ratio of 76.2:23.8	*SLM* Laser power: 80 W Scan speed: 100–400 mm/s Scan spacing: 50 μm Layer thickness: 50 μm	In situ formed TiC is found within Ti_5Si_3 Maximum densification is achieved at 0.4 kJ/m of laser energy density Optimum density is 96.9% theoretical density, mircohardness is $980.3HV_{0.2}$, which is 300% higher than unreinforced Ti part COF is 0.2 and wear rate is reduced to 1.42×10^{-4} mm^3/Nm At higher laser energy density, COF and wear rate increase due to coarsened dendrites of TiC reinforcing phase, and low densification rate
Zheng et al. [89]	Ti6Al4V (82 μm) and 10–20 wt % Ni-coated TiC (36 μm)	*LMD* Laser power: 240 W Scan spacing: 380 μm Layer thickness: 250 μm Scan speed: 14.8 mm/s Powder feed rate: 10 g/min	Melting and re-solidification of TiC particles result in fine microstructure as well as stronger reinforcement/matrix interface bonding The composite shows significantly higher strength and isotropic properties, compared to the monolithic matrix alloy. The compressive yield strength is improved from 970 to 1950 MPa The ductility of composite is lowered to about 2% Ti–Ni intermetallic phase contributes to strength improvement but is harmful to ductility Grain size is refined
Mahamood et al. [90]	Ti6Al4V (150–200 μm) and TiC (< 60 μm)	*LMD* Laser power: 3.2 kW Powder flow rate: 2.88 g/min Scan speed: 0.015–0.105 m/s	Scan speed is critical in controlling physical, mechanical, metallurgical, and tribological properties of the MMC Optimum scan speed is 0.065 m/s, which gives best wear resistance
Gu et al. [91]	Ti (22.5 μm) and 15 wt% TiC (50 nm)	*SLM* Laser power: 200 W Spot size: 70 μm Layer thickness: 50 μm Scan speed: 0.1–0.4 m/s Scan spacing: 50 μm	Densification level remains above 97% as the volumetric energy density increases over 120 J/mm^3 Microhardness and elastic modulus experience 22.7-fold and 2.4-fold increase compared to the unreinforced Ti
Ochonogor et al. [92]	Ti6Al4V (45–75 μm) and 10–40 wt%TiC (32–45 μm)	*LMD* Laser power: 750 W Scan speed: 10 mm/s Powder federate: Ti6Al4V 1.3–2.2 g/min, TiC 0.3–1.2 g/min	Dispersion of TiC in matrix is homogenous, free of cracks and pores At 40 wt% TiC addition, microhardness is improved from 357 $HV_{0.1}$ to 922.2 $HV_{0.1}$ Wear resistance of the material is improved significantly, resulting in 15-fold wear rate reduction

Table 5 continued

Authors	Materials/preparation	Laser processing parameters	Effects/Improvements/findings
Gu et al. [93]	Ti (22.5 μm) and 7.5–22.5 wt% TiC (50 nm)	*SLM* Laser power: 90 W Spot size: 70 μm Scan speed: 0.3 m/s Scan spacing: 50 μm Layer thickness: 50 μm	The optimal TiC content is determined to be 12.5 wt% The composite shows a density of 98.3% The microhardness is elevated to $577HV_{0.2}$, and COF is lowered to 0.19
Liu et al. [94]	TA15 and 10 wt% TiC	*LMD* Laser power: 3.5–4 kW Spot size: 5 mm Powder feed rate: 7.5–8.8 g/min	The TiC particles dissolve during laser melting and precipitate during cooling The composite has superior creep resistance to the monolithic alloy Particle agglomeration can still be found
Zhang et al. [95]	Ti and 5–40 vol% TiC (both 75–150 μm)	*LMD* Laser power: 1.5–2.1 kW Scan speed: 3–4 mm/s	The tensile strength of the composite changes marginally with TiC content, while the ductility shows a sharp decrease with the increase in TiC addition Functional gradient material without a discrete interface could be obtained through this process
Obielodan & Stucker [96]	Ti6Al4V (125–210 μm) and (0–10 wt%) TiC (45–150 μm)	*LENS* Laser power: 200–270 W Layer thickness: 250 μm Scan spacing: 380 μm	Functional gradient composite material is fabricated with different designs of material transition The mode of transition from one material to another has significant effect on tensile strength
Attar et al. [98]	Ti (48.69 μm) and 5 wt% TiB_2 (3.5–6 μm)	*SLM* Laser power: 180 W Scan speed: 150 mm/s Scan spacing: 100 μm Layer thickness: 100 μm	Chemical reaction between Ti and TiB_2 occurs, leading to the formation of Ti–TiB composite The mechanical property of SLM-produced composite shows comparable mechanical properties to samples made by casting
Farayibi et al. [100]	Ti6Al4V and 68–76 wt% WC	*Laser cladding* Laser power: 1400–1800 W Scan speed: 200–400 mm/min Powder feed rate: 10–30 g/min	Nano-sized products (TiC and W) uniformly distributes within the matrix The composite with 76 wt% WC offers resistance to erosion up to 13 times that of wrought Ti6Al4V component

high reflectivity of the laser source, high oxidization tendency, and the high thermal conductivity of aluminum result in significant obstacles for additive manufacturing [108]. Besides, the relatively poor surface finish achievable with laser-assisted AM constitutes a major challenge. The high surface roughness and existence of open pores on the surface deteriorate both the fatigue properties and the corrosion resistance of AM processed metallic parts. In addition, for laser-assisted AM, the large variations in microstructure may lead to the inconsistency in mechanical properties. As such, addressing those general challenges represents the exciting research opportunities for AM-produced MMCs.

Defect mitigation and control

Although various AM-produced MMCs have been demonstrated in the literature, the performance of the MMCs in general is not on par with that of traditional MMCs, mainly due to the natural weaknesses of the laser-assisted AM processes. For instance, the laser-assisted AM processes often result in a degree of porosity, which generally is detrimental to the mechanical properties and service life of components. It is well understood that the existence of pores deteriorates material strength, ductility, and fatigue properties [109]. If no compression is used, laser-sintered materials are usually porous [110]. Controlling parameters of the laser-assisted AM process, such as scan speed (exposure time) [111] and laser power [112], are found to significantly affect the

porosity of products. In the literature, optimization of AM process parameters for regular metal alloys is well documented. However, such effort has been lacking for AM-produced MMCs. One should expect that the optimal process parameters for a metal alloy may not be the optimal for the MMCs with such an alloy as the matrix material. Meanwhile, a number of studies have also confirmed that the addition of reinforcement particles into metal matrix during laser-assisted AM process will result in higher porosity and reduce material ductility [14, 42, 53]. This certainly makes the optimization of AM process parameters more challenging. As such, it is believed that more research efforts are expected to achieve low material porosity of the laser-assisted AM-produced MMCs. Also, other common defects including deformation, detrimental residual stress, and surface roughness have been extensively investigated and discussed for the AM-produced metal alloys, but the effort has still been lacking for AM-produced MMCs. For those defects, the formation mechanism and mitigation strategies should be developed for AM-produced MMCs. In this regard, research is also called for to compare different laser-assisted AM processes in terms of defect mitigation and performance improvement. Industry has been particularly interested in learning the differences among the AM processes in producing MMCs, and thus, proper technical and business decisions can be made.

MMC reinforcements for laser-assisted AM

Future research should also investigate the suitability of other advanced reinforcement materials in laser-assisted AM of MMCs. Most studies reviewed in this paper adopt particulate reinforcements. However, other types of reinforcement, such as platelets, whiskers, or fibers, have different reinforcing mechanisms when introduced into metal matrix material, and they could also significantly enhance material performance under specific loading circumstances. Those reinforcements are frequently adopted in conventional manufacturing of MMCs, but they have been hardly investigated in laser-assisted AM processes. Meanwhile, the difficulty of achieving good wettability between the reinforcing particles and matrix is also regarded as a major obstacle [39, 41, 42]. Therefore, the development of new reinforcement material, as well as infiltrant materials with higher permeability and bondability with matrix

materials, is urgently called for. This is particularly true for the laser-assisted AM processes where the extremely short process cycle is generally not favorable for diffusion. Also, the interaction between the reinforcements and the laser during laser-assisted AM of MMCs deserves significant research attention. There are many unknown phenomena in the process such as decomposition and vaporization of reinforcement particle, and understanding the phenomena will greatly help the microstructure and mechanical properties of the AM-produced MMCs. In addition, the geometry and size effects of the raw matrix and reinforcement particles are rarely studied in laser-assisted AM of MMCs, while these parameters are confirmed critical to product porosity and microstructure in conventional powder metallurgy [113–115].

Dispersion of reinforcements

The processing techniques of making MMCs also possess a major opportunity for improvement. One technical challenge of manufacturing MMC via laser-assisted AM techniques may be the difficulty of achieving a uniform distribution of particles, especially when nano-sized reinforcing particles are adopted. Agglomeration of reinforcing particles has been reported in many studies, and this limits the performance of final MMC products [34, 52, 74]. As investigated, mechanical mixing (e.g., ball milling, liquid state stirring) is the most adopted method to prepare raw powder mixture for making MMCs via laser-assisted AM. These methods may have a detrimental effect on particle morphology, introduce impurities, and lead to limited dispersing effect. Meanwhile, various powder mixing methods are proposed in conventional powder metallurgy, such as ultrasonic processing, particle surface modification, addition of dispersing agent, and applying external magnetic field. Therefore, more efficient particles dispersion techniques are expected to reduce the agglomeration of nano-sized reinforcement particles in laser-assisted AM processes.

There is another level of complexity in achieving uniform dispersion of reinforcing particles in laser-assisted AM processes. In PBF processes, the spreading of a fresh layer of powder by a recoating mechanism may alter the dispersion of reinforcement in the matrix powders, and in turn affect the final dispersion in the MMC. In DED processes, powder

mixture is transported from a powder feeder, going through the deposition head, to exist the nozzle. The powder transport will certainly change the dispersion of reinforcement in the matrix. In this regard, both issues represent challenges, and they will need to be investigated to improve the uniform dispersion of reinforcement. Besides, the possible redistribution of reinforcement due to laser material interaction and raid solidification during laser-assisted AM processes should also be studied [116].

Post-processing

Moreover, due to the nature of laser-assisted AM processes, the as-built components have been plagued by challenging issues such as high porosity, high gradient residual stress, geometry distortion, and low surface quality. Post-treatment is reasonably expected to mitigate these negative effects and improve components performance. The research on post-treating AM-produced regular metal alloys is abundant—various methods of heat treatment, hot isostatic pressing, ultrasonic peening, laser shock peening, mechanical rolling, and machining have been attempted. However, the research on post-treating AM-produced MMCs has been lagging behind. As such, the adoption of post-treatments, for homogenizing microstructure, improving matrix/reinforcement interface, and reducing the porosity of laser-assisted AM-produced MMCs, should be explored. Finally, from a systematic point of view, laser-assisted AM process has proven to be economically inefficient requiring costly raw powder preparation and expensive post-processing. In order to effectively reduce the cost and realize the industrial applications of laser-assisted AM techniques, further investigation is required to lower the cost of raw powder preparation and post-processing.

Modeling and simulation

In order to understand the material melting/solidification, matrix/reinforcement interaction, as well as residual stress and defects formation during laser-assisted AM processes, modeling and simulation is regarded as another indispensable research area. For laser-assisted AM processes, the rapid thermal cycle and localized melting/solidification create major challenges to any in situ observation approaches. Modeling efforts at atomistic, micro-, meso-, and macro-levels are all appreciated. With reliable predictive models, the fundamental mechanisms can be understood, and thus, the laser-assisted AM process for making MMCs can be optimized. As a result, the costly trial-and-error experiments can be minimized. In this regard, serious challenges still exist in developing the predictive thermo-mechanical models for the various sub-processes during the laser-assisted AM processes, including temporal material property change, microstructure evolution, matrix/reinforcement interaction, and precipitate formation. Moreover, the current design of MMC systems is primarily based on the trial-and-error mechanism, which is time-consuming and costly. Thus, advanced predictive methods such as Calphad (calculation of phase diagram) are expected t be more actively adopted in the future design of new MMC material systems.

Conclusions

Development of MMCs by laser-assisted AM techniques is a promising area for both academia and industry. In recent years, significant efforts have been made to obtain various MMCs, primarily by powder bed fusion (PBF) processes and directed energy deposition (DED) processes. This paper surveys those developments. To the best of our knowledge, this is the first comprehensive review on this topic. The reviewed research works are categorizes based on the types of metal matrix materials, namely, aluminum/aluminum alloys, copper/copper alloys, iron/iron alloys, nickel/nickel alloys, titanium/titanium alloys, and other types of metals. The microstructure and resultant properties especially mechanical properties are summarized, and the findings of these studies are thoroughly summarized and compared. It is indicated that although strengthening AM-produced metal parts using second phase materials is promising, there still exist significant challenges and limitations for MMCs processed via laser-assisted AM methods. By providing such a critical analysis on the existing literature, the future research opportunities are pointed out. It is hoped that this comprehensive review will stimulate more exciting research to address the fundamental scientific problems and develop understanding for industry to adopt laser-assisted AM to produce MMCs with confidence.

Acknowledgements

Compliance with ethical standards

Conflict of interest The authors declare that they have no conflict of interest.

References

[1] Ibrahim IA, Mohamed FA, Lavernia EJ (1991) Particulate reinforced metal matrix composites: a review. J Mater Sci 26:1137–1156. https://doi.org/10.1007/BF00544448

[2] Chawla N, Shen YL (2001) Mechanical behavior of particle reinforced metal matrix composites. Adv Eng Mater 3:357–370. https://doi.org/10.1002/1527-2648(200106)3:6%3c357:AID-ADEM357%3e3.0.CO;2-I

[3] Cyriac AJ (2011) Metal matrix composites: history, status, factors and future (Doctoral dissertation, Oklahoma State University)

[4] Qu XH, Zhang L, Wu M, Bin RS (2011) Review of metal matrix composites with high thermal conductivity for thermal management applications. Prog Nat Sci Mater Int 21:189–197. https://doi.org/10.1016/S1002-0071(12)60029-X

[5] Campbell I, Diegel O, Kowen J, Wohlers T (2019) Wohlers Report 2019: 3D printing and additive manufacturing state of the industry: annual worldwide progress report, Wohlers Associates

[6] Standard A (2013) F2792-12a: standard terminology for additive manufacturing technologies (ASTM International, West Conshohocken, PA, 2012). P Jain, AM Kuthe, Feasibility study Manuf using rapid Prototyp FDM approach. Procedia Eng 63:4–11

[7] Bhavar V, Kattire P, Patil V et al (2017) A review on powder bed fusion technology of metal additive manufacturing. In: Additive manufacturing handbook, CRC Press, Boca Raton, pp 251–253

[8] Sercombe TB, Li X (2016) Selective laser melting of aluminium and aluminium metal matrix composites. Mater Technol 31:77–85. https://doi.org/10.1179/1753555715Y.0000000078

[9] Song B, Dong S, Coddet P et al (2013) Microstructure and tensile behavior of hybrid nano-micro SiC reinforced iron matrix composites produced by selective laser melting. J Alloys Compd 579:415–421. https://doi.org/10.1016/j.jallcom.2013.06.087

[10] Xavior MA (2014) Graphene reinforced metal matrix composite (GRMMC): a review. In: Procedia engineering, Vellore, India, pp 1033–1040

[11] Jiang J, He X, Du J et al (2018) In-situ fabrication of graphene-nickel matrix composites. Mater Lett 220:178–181. https://doi.org/10.1016/j.matlet.2018.03.039

[12] Ghosh SK, Saha P, Kishore S (2010) Influence of size and volume fraction of SiC particulates on properties of ex situ reinforced Al–4.5Cu–3 Mg metal matrix composite prepared by direct metal laser sintering process. Mater Sci Eng, A 527:4694–4701. https://doi.org/10.1016/j.msea.2010.03.108

[13] Simchi A, Godlinski D (2008) Effect of SiC particles on the laser sintering of Al–7Si–0.3 Mg alloy. Scr Mater 59:199–202. https://doi.org/10.1016/j.scriptamat.2008.03.007

[14] Manfredi D, Calignano F, Krishnan M et al (2014) Additive manufacturing of Al alloys and aluminium matrix composites (AMCs). Light Met Alloy Appl 11:3–34. https://doi.org/10.5772/57069

[15] Gu D, Chang F, Dai D (2015) Selective laser melting additive manufacturing of novel aluminum based composites with multiple reinforcing phases. J Manuf Sci Eng. https://doi.org/10.1115/1.4028925

[16] Gu D, Wang H, Dai D et al (2015) Rapid fabrication of Al-based bulk-form nanocomposites with novel reinforcement and enhanced performance by selective laser melting. Scr Mater 96:25–28. https://doi.org/10.1016/j.scriptamat.2014.10.011

[17] Gu D, Wang H, Dai D et al (2015) Densification behavior, microstructure evolution, and wear property of TiC nanoparticle reinforced AlSi10Mg bulk-form nanocomposites prepared by selective laser melting. J Laser Appl 27:S17003. https://doi.org/10.2351/1.4870877

[18] Dubourg L, Ursescu D, Hlawka F, Cornet A (2005) Laser cladding of MMC coatings on aluminium substrate: influence of composition and microstructure on mechanical properties. Wear 258:1745–1754. https://doi.org/10.1016/j.wear.2004.12.010

[19] Dadbakhsh S, Hao L (2012) Effect of hot isostatic pressing (HIP) on Al composite parts made from laser consolidated Al/Fe$_2$O$_3$ powder mixtures. J Mater Process Technol 212:2474–2483. https://doi.org/10.1016/j.jmatprotec.2012.06.016

[20] Dadbakhsh S, Hao L, Jerrard PGE, Zhang DZ (2012) Experimental investigation on selective laser melting behaviour and processing windows of in situ reacted Al/Fe$_2$O$_3$ powder mixture. Powder Technol 231:112–121. https://doi.org/10.1016/j.powtec.2012.07.061

[21] Han Q, Setchi R, Lacan F et al (2017) Selective laser melting of advanced Al-Al$_2$O$_3$ nanocomposites: simulation, microstructure and mechanical properties. Mater Sci Eng, A 698:162–173. https://doi.org/10.1016/j.msea.2017.05.061

[22] Sercombe TB, Schaffer GB (2004) On the role of tin in the infiltration of aluminium by aluminium for rapid prototyping applications. Scr Mater 51:905–908. https://doi.org/10.1016/j.scriptamat.2004.06.032

[23] Yu P, Schaffer GB (2009) Microstructural evolution during pressureless infiltration of aluminium alloy parts fabricated by selective laser sintering. Acta Mater 57:163–170. https://doi.org/10.1016/j.actamat.2008.08.065

[24] Dai D, Gu D (2016) Influence of thermodynamics within molten pool on migration and distribution state of reinforcement during selective laser melting of AlN/AlSi10Mg composites. Int J Mach Tools Manuf 100:14–24. https://doi.org/10.1016/j.ijmachtools.2015.10.004

[25] Li XP, Ji G, Chen Z et al (2017) Selective laser melting of nano-TiB2 decorated AlSi10Mg alloy with high fracture strength and ductility. Acta Mater 129:183–193. https://doi.org/10.1016/j.actamat.2017.02.062

[26] Famodimu OH, Stanford M, Oduoza CF, Zhang L (2018) Effect of process parameters on the density and porosity of laser melted AlSi10Mg/SiC metal matrix composite. Front Mech Eng 13:520–527. https://doi.org/10.1007/s11465-018-0521-y

[27] Jiang LY, Liu TT, Zhang CD et al (2018) Preparation and mechanical properties of CNTs-AlSi10Mg composite fabricated via selective laser melting. Mater Sci Eng, A 734:171–177. https://doi.org/10.1016/j.msea.2018.07.092

[28] Zhao X, Song B, Fan W et al (2016) Selective laser melting of carbon/AlSi10Mg composites: microstructure, mechanical and electronical properties. J Alloys Compd 665:271–281. https://doi.org/10.1016/j.jallcom.2015.12.126

[29] Wang Y, Shi J, Lu S, Xiao W (2018) Investigation of porosity and mechanical properties of graphene nanoplatelets-reinforced AlSi10 Mg by selective laser melting. J Micro Nano-Manuf 6:10902. https://doi.org/10.1115/1.4038454

[30] Slocombe A, Li L (2001) Selective laser sintering of TiC-Al$_2$O$_3$ composite with self-propagating high-temperature synthesis. J Mater Process Technol 118:173–178. https://doi.org/10.1016/S0924-0136(01)00905-0

[31] Ghosh SK, Saha P (2011) Crack and wear behavior of SiC particulate reinforced aluminium based metal matrix composite fabricated by direct metal laser sintering process. Mater Des 32:139–145. https://doi.org/10.1016/j.matdes.2010.06.020

[32] Uhlmann E, Piltz S, Schauer K (2005) Micro milling of sintered tungsten–copper composite materials. J Mater Process Technol 167:402–407. https://doi.org/10.1016/j.jmatprotec.2005.05.022

[33] Pintsuk G, Brünings SE, Döring JE et al (2003) Development of W/Cu-functionally graded materials. Fusion Eng Des 66:237–240. https://doi.org/10.1016/S0920-3796(03)00220-5

[34] Gu D, Shen Y (2006) WC-Co particulate reinforcing Cu matrix composites produced by direct laser sintering. Mater Lett 60:3664–3668. https://doi.org/10.1016/j.matlet.2006.03.103

[35] Gu DD, Shen YF, Dai P, Yang MC (2006) Microstructure and property of sub-micro WC-10%Co particulate reinforced Cu matrix composites prepared by selective laser sintering. Trans Nonferrous Met Soc China 16:357–362. https://doi.org/10.1016/S1003-6326(06)60061-7

[36] Gu D, Shen Y (2009) Microstructures and properties of direct laser sintered tungsten carbide (WC) particle reinforced Cu matrix composites with RE–Si–Fe addition: a comparative study. J Mater Res 24:3397–3406. https://doi.org/10.1557/jmr.2009.0419

[37] Gu D, Shen Y, Zhao L et al (2007) Effect of rare earth oxide addition on microstructures of ultra-fine WC-Co particulate reinforced Cu matrix composites prepared by direct laser sintering. Mater Sci Eng, A 445:316–322. https://doi.org/10.1016/j.msea.2006.09.057

[38] Agarwala MK, Bourell DL, Wu B, Beaman JJ (1993) An evaluation of the mechanical behavior of bronze-Ni composites produced by selective laser sintering. In: Solid freeform fabrication symposium, Austin, Texas, USA

[39] Gu D, Shen Y, Lu Z (2009) Microstructural characteristics and formation mechanism of direct laser-sintered Cu-based alloys reinforced with Ni particles. Mater Des 30:2099–2107. https://doi.org/10.1016/j.matdes.2008.08.036

[40] Dürr H, Pilz R, Eleser NS (1999) Rapid tooling of EDM electrodes by means of selective laser sintering. Comput Ind 39:35–45. https://doi.org/10.1016/S0166-3615(98)00123-7

[41] Lu L, Fuh JYH, Chen ZD et al (2000) In situ formation of TiC composite using selective laser melting. Mater Res Bull 35:1555–1561. https://doi.org/10.1016/S0025-5408(00)00339-1

[42] Leong CC, Lu L, Fuh JYH, Wong YS (2002) In-situ formation of copper matrix composites by laser sintering. Mater Sci Eng, A 338:81–88. https://doi.org/10.1016/S0921-5093(02)00050-3

[43] Hu Z, Chen F, Lin D et al (2017) Laser additive manufacturing bulk graphene–copper nanocomposites.

Nanotechnology 28:445705. https://doi.org/10.1088/1361-6528/aa8946

[44] Spierings AB, Leinenbach C, Kenel C, Wegener K (2014) Processing of metal-diamond-composites using selective laser melting. In: Solid freeform fabrication proceedings, Austin, Texas, USA, pp 764–774

[45] Liu JH, Shi YS, Chen KH, Huang SH (2007) Research on manufacturing Cu matrix Fe–Cu–Ni–C alloy composite parts by indirect selective laser sintering. Int J Adv Manuf Technol 33:693–697. https://doi.org/10.1007/s00170-006-0493-7

[46] Dück J, Niebling F, Neeße T, Otto A (2004) Infiltration as post-processing of laser sintered metal parts. Powder Technol 145:62–68. https://doi.org/10.1016/j.powtec.2004.05.006

[47] Khaing MW, Fuh JYH, Lu L (2001) Direct metal laser sintering for rapid tooling: processing and characterisation of EOS parts. J Mater Process Technol 113:269–272. https://doi.org/10.1016/S0924-0136(01)00584-2

[48] Zhu HH, Lu L, Fuh JYH (2003) Development and characterisation of direct laser sintering Cu-based metal powder. J Mater Process Technol 140:314–317. https://doi.org/10.1016/S0924-0136(03)00755-6

[49] Song B, Dong S, Liao H, Coddet C (2013) Characterisations of TiC particle reinforced FeAl composite part fabricated by selective laser melting. Mater Res Innov 18:50–56. https://doi.org/10.1179/1433075x13y.0000000127

[50] Emamian A, Alimardani M, Khajepour A (2012) Correlation between temperature distribution and in situ formed microstructure of Fe-TiC deposited on carbon steel using laser cladding. Appl Surf Sci 258:9025–9031. https://doi.org/10.1016/j.apsusc.2012.05.143

[51] Emamian A, Alimardani M, Khajepour A (2015) Effect of cooling rate and laser process parameters on additive manufactured Fe-Ti-C metal matrix composites microstructure and carbide morphology. J Manuf Process 16:511–517. https://doi.org/10.1016/j.jmapro.2014.07.002

[52] Biedunkiewicz A, Biedunkiewicz W, Grzesiak D, Figiel P (2012) Mechanical properties of NC-TiB2/steel and NC-TiC/steel composite synthesized by selective laser melting. In: ECCM 15th European conference on composite material, Venice, Italy, pp 24–28

[53] Gåård A, Krakhmalev P, Bergström J (2006) Microstructural characterization and wear behavior of (Fe, Ni)-TiC MMC prepared by DMLS. J Alloys Compd 421:166–171. https://doi.org/10.1016/j.jallcom.2005.09.084

[54] Amano RS, Marek S, Schultz BF, Rohatgi PK (2014) Laser engineered net shaping process for 316 l/15% nickel coated titanium carbide metal matrix composite. J Manuf Sci Eng 136:051007. https://doi.org/10.1115/1.4027758

[55] Alimardani M, Emamian A, Khajepour A, Corbin SF (2010) The effect of thermal field on the deposition of Fe-TiC on carbon steel using laser cladding. In: ASME 2010 international mechanical engineering congress and exposition, Vancouver, British Columbia, Canada, pp 11–18

[56] Ramesh CS, Srinivas CK, Channabasappa BH (2009) Abrasive wear behaviour of laser sintered iron-SiC composites. Wear 267:1777–1783. https://doi.org/10.1016/j.wear.2008.12.026

[57] Ramesh CS, Srinivas CK (2009) Friction and wear behavior of laser-sintered iron-silicon carbide composites. J Mater Process Technol 209:5429–5436. https://doi.org/10.1016/j.jmatprotec.2009.04.018

[58] Lin D, Ye C, Liao Y et al (2013) Mechanism of fatigue performance enhancement in a laser sintered superhard nanoparticles reinforced nanocomposite followed by laser shock peening. J Appl Phys 113:133509. https://doi.org/10.1063/1.4799154

[59] Kang N, Ma W, Li F et al (2018) Microstructure and wear properties of selective laser melted WC reinforced 18Ni-300 steel matrix composite. Vacuum 154:69–74. https://doi.org/10.1016/j.vacuum.2018.04.044

[60] Yan X, Huang C, Chen C et al (2018) Additive manufacturing of WC reinforced maraging steel 300 composites by cold spraying and selective laser melting. Surf Coat Technol 371:161–171. https://doi.org/10.1016/j.surfcoat.2018.03.072

[61] AlMangour B, Grzesiak D, Yang J-M (2016) Rapid fabrication of bulk-form TiB2/316L stainless steel nanocomposites with novel reinforcement architecture and improved performance by selective laser melting. J Alloys Compd 680:480–493. https://doi.org/10.1016/j.jallcom.2016.04.156

[62] Zheng Z, Wang L, Jia M et al (2017) Microstructure and mechanical properties of stainless steel/calcium silicate composites manufactured by selective laser melting. Mater Sci Eng, C 71:1099–1105. https://doi.org/10.1016/j.msec.2016.11.032

[63] Dewidar MM, Dalgarno KW, Wright CS (2003) Processing conditions and mechanical properties of high-speed steel parts fabricated using direct selective laser sintering. Proc Inst Mech Eng Part B J Eng Manuf 217:1651–1663. https://doi.org/10.1243/095440503772680587

[64] Kumar S, Kruth JP (2007) Effect of bronze infiltration into laser sintered metallic parts. Mater Des 282:400–407. https://doi.org/10.1016/j.matdes.2005.09.016

[65] Yan C, Shi Y, Yang J, Liu J (2009) Preparation and selective laser sintering of nylon-12 coated metal powders and post processing. J Mater Process Technol 209:5785–5792. https://doi.org/10.1016/j.jmatprotec.2009.06.010

[66] Liu J, Shi Y, Lu Z et al (2006) Rapid manufacturing metal parts by laser sintering admixture of epoxy resin/iron powders. Adv Eng Mater 8:988–994. https://doi.org/10.1002/adem.200600060

[67] Simchi A, Pohl H (2004) Direct laser sintering of iron-graphite powder mixture. Mater Sci Eng, A 383:191–200. https://doi.org/10.1016/j.msea.2004.05.070

[68] Lin D, Richard Liu C, Cheng GJ (2014) Single-layer graphene oxide reinforced metal matrix composites by laser sintering: microstructure and mechanical property enhancement. Acta Mater 80:183–193. https://doi.org/10.1016/j.actamat.2014.07.038

[69] Cooper DE, Blundell N, Maggs S, Gibbons GJ (2013) Additive layer manufacture of Inconel 625 metal matrix composites, reinforcement material evaluation. J Mater Process Technol 213:2191–2200. https://doi.org/10.1016/j.jmatprotec.2013.06.021

[70] Hong C, Gu D, Dai D et al (2015) High-temperature oxidation performance and its mechanism of TiC/Inconel 625 composites prepared by laser metal deposition additive manufacturing. J Laser Appl 27:S17005. https://doi.org/10.2351/1.4898647

[71] Bi G, Sun CN, Nai ML, Wei J (2013) Micro-structure and mechanical properties of nano-TiC reinforced Inconel 625 deposited using LAAM. Phys Procedia 41:828–834. https://doi.org/10.1016/j.phpro.2013.03.155

[72] Hong C, Gu D, Dai D et al (2013) Laser metal deposition of TiC/Inconel 718 composites with tailored interfacial microstructures. Opt Laser Technol 54:98–109. https://doi.org/10.1016/j.optlastec.2013.05.011

[73] Gu D, Hong C, Jia Q et al (2013) Combined strengthening of multi-phase and graded interface in laser additive manufactured TiC/Inconel 718 composites. J Phys D Appl Phys 47:45309. https://doi.org/10.1088/0022-3727/47/4/045309

[74] Jia Q, Gu D (2014) Selective laser melting additive manufacturing of Inconel 718 superalloy parts: densification, microstructure and properties. J Alloys Compd 585:713–721. https://doi.org/10.1016/j.jallcom.2013.09.171

[75] Wilson JM, Shin YC (2012) Microstructure and wear properties of laser-deposited functionally graded Inconel 690 reinforced with TiC. Surf Coat Technol 207:517–522. https://doi.org/10.1016/j.surfcoat.2012.07.058

[76] Cui C, Guo Z, Wang H, Hu J (2007) In situ TiC particles reinforced grey cast iron composite fabricated by laser cladding of Ni-Ti-C system. J Mater Process Technol 183:380–385. https://doi.org/10.1016/j.jmatprotec.2006.10.031

[77] Zheng B, Topping T, Smugeresky JE et al (2010) The influence of Ni-coated TiC on laser-deposited IN625 metal matrix composites. Metall Mater Trans A Phys Metall Mater Sci 41:568–573. https://doi.org/10.1007/s11661-009-0126-5

[78] Wang Y, Shi J (2020) Effect of post heat treatment on the microstructure and tensile properties of nano TiC particulate reinforced Inconel 718 by selective laser melting. J Manuf Sci Eng. https://doi.org/10.1115/1.4046646

[79] Rong T, Gu D, Shi Q et al (2016) Effects of tailored gradient interface on wear properties of WC/Inconel 718 composites using selective laser melting. Surf Coat Technol 307:418–427. https://doi.org/10.1016/j.surfcoat.2016.09.011

[80] Nguyen QB, Zhu Z, Chua BW et al (2018) Development of WC-Inconel composites using selective laser melting. Arch Civ Mech Eng 18:1410–1420. https://doi.org/10.1016/j.acme.2018.05.001

[81] Zhang B, Bi G, Nai S et al (2016) Microhardness and microstructure evolution of TiB2 reinforced Inconel 625/TiB2 composite produced by selective laser melting. Opt Laser Technol 80:186–195. https://doi.org/10.1016/j.optlastec.2016.01.010

[82] Wang Y, Shi J, Lu S, Wang Y (2017) Selective laser melting of graphene-reinforced Inconel 718 superalloy: evaluation of microstructure and tensile performance. J Manuf Sci Eng. https://doi.org/10.1115/1.4034712

[83] Xiao W, Lu S, Wang Y, Jing SHI (2018) Mechanical and tribological behaviors of graphene/Inconel 718 composites. Trans Nonferrous Met Soc China 28:1958–1969. https://doi.org/10.1016/S1003-6326(18)64841-1

[84] Wang Y, Shi J (2020) Microstructure and tensile performance of graphene-reinforced Inconel 718 alloy via selective laser melting and post-treatments. J Micro Nano-Manuf. https://doi.org/10.1115/1.4045765

[85] Attar H, Ehtemam-Haghighi S, Kent D, Dargusch MS (2018) Recent developments and opportunities in additive manufacturing of titanium-based matrix composites: a review. Int J Mach Tools Manuf 133:85–102. https://doi.org/10.1016/j.ijmachtools.2018.06.003

[86] Gu D, Wang Z, Shen Y et al (2009) In-situ TiC particle reinforced Ti-Al matrix composites: powder preparation by mechanical alloying and selective laser melting behavior. Appl Surf Sci 255:9230–9240. https://doi.org/10.1016/j.apsusc.2009.07.008

[87] Zhang Y, Sun J, Vilar R (2011) Characterization of (TiB + TiC)/TC4 in situ titanium matrix composites prepared by laser direct deposition. J Mater Process Technol. https://doi.org/10.1016/j.jmatprotec.2010.11.009

[88] Gu D, Hagedorn YC, Meiners W et al (2011) Selective laser melting of in situ TiC/Ti5Si3 composites with novel reinforcement architecture and elevated performance. Surf Coat

Technol 205:3285–3292. https://doi.org/10.1016/j.surfcoat.2010.11.051

[89] Zheng B, Smugeresky JE, Zhou Y et al (2008) Microstructure and properties of laser-deposited Ti6Al4 V metal matrix composites using Ni-Coated powder. Metall Mater Trans A Phys Metall Mater Sci 39:1196–1205. https://doi.org/10.1007/s11661-008-9498-1

[90] Mahamood RM, Akinlabi ET, Shukla M, Pityana S (2013) Scanning velocity influence on microstructure, microhardness and wear resistance performance of laser deposited Ti6Al4 V/TiC composite. Mater Des 50:656–666. https://doi.org/10.1016/j.matdes.2013.03.049

[91] Gu D, Hagedorn YC, Meiners W et al (2011) Nanocrystalline TiC reinforced Ti matrix bulk-form nanocomposites by selective laser melting (SLM): densification, growth mechanism and wear behavior. Compos Sci Technol 71:1612–1620. https://doi.org/10.1016/j.compscitech.2011.07.010

[92] Ochonogor OF, Meacock C, Abdulwahab M et al (2012) Effects of Ti and TiC ceramic powder on laser-cladded Ti-6Al-4V in situ intermetallic composite. Appl Surf Sci 263:591–596. https://doi.org/10.1016/j.apsusc.2012.09.114

[93] Gu D, Meng G, Li C et al (2012) Selective laser melting of TiC/Ti bulk nanocomposites: influence of nanoscale reinforcement. Scr Mater 67:185–188. https://doi.org/10.1016/j.scriptamat.2012.04.013

[94] Liu D, Zhang SQ, Li A, Wang HM (2010) Creep rupture behaviors of a laser melting deposited TiC/TA15 in situ titanium matrix composite. Mater Des 31:3127–3133. https://doi.org/10.1016/j.matdes.2009.12.036

[95] Zhang Y, Wei Z, Shi L, Xi M (2008) Characterization of laser powder deposited Ti-TiC composites and functional gradient materials. J Mater Process Technol 206:438–444. https://doi.org/10.1016/j.jmatprotec.2007.12.055

[96] Obielodan J, Stucker B (2013) Characterization of LENS-fabricated Ti6Al4V and Ti6Al4V/TiC dual-material transition joints. Int J Adv Manuf Technol 66:2053–2061. https://doi.org/10.1007/s00170-012-4481-9

[97] Shishkovsky I, Kakovkina N, Sherbakov V (2017) Graded layered titanium composite structures with TiB2 inclusions fabricated by selective laser melting. Compos Struct 169:90–96. https://doi.org/10.1016/j.compstruct.2016.11.013

[98] Attar H, Bönisch M, Calin M et al (2014) Comparative study of microstructures and mechanical properties of in situ Ti-TiB composites produced by selective laser melting, powder metallurgy, and casting technologies. J Mater Res 29:1941–1950. https://doi.org/10.1557/jmr.2014.122

[99] Attar H, Bönisch M, Calin M et al (2014) Selective laser melting of in situ titanium-titanium boride composites: processing, microstructure and mechanical properties. Acta Mater 76:13–22. https://doi.org/10.1016/j.actamat.2014.05.022

[100] Farayibi PK, Murray JW, Huang L et al (2014) Erosion resistance of laser clad Ti-6Al-4V/WC composite for waterjet tooling. J Mater Process Technol 214:710–721. https://doi.org/10.1016/j.jmatprotec.2013.08.014

[101] Sun CN, Baldridge T, Gupta MC (2009) Fabrication of ZrB2-Zr cermet using laser sintering technique. Mater Lett 63:2529–2531. https://doi.org/10.1016/j.matlet.2009.08.059

[102] Ochonogor OF, Meacock C, Pityana SL et al (2012) Microstructure characterization of laser-deposited titanium carbide and zirconium-based titanium metal matrix composites. J S Afr Inst Min Metall 112:905–910

[103] Liu DM, Si TZ, Wang CC, Zhang QA (2007) Phase component, microstructure and hydrogen storage properties of the laser sintered Mg-20 wt% LaNi5 composite. Scr Mater 57:389–392. https://doi.org/10.1016/j.scriptamat.2007.05.011

[104] Si TZ, Zhang QA (2006) Phase structures and electrochemical properties of the laser sintered LaNi5-x wt% Mg2Ni composites. J Alloys Compd 414:317–321. https://doi.org/10.1016/j.jallcom.2005.07.040

[105] Li C, Liu ZY, Fang XY, Guo YB (2018) Residual stress in metal additive manufacturing. Procedia CIRP 71:348–353. https://doi.org/10.1016/j.procir.2018.05.039

[106] Megahed M, Mindt H-W, N'Dri N et al (2016) Metal additive-manufacturing process and residual stress modeling. Integr Mater Manuf Innov 5:61–93. https://doi.org/10.1186/s40192-016-0047-2

[107] Denlinger ER, Heigel JC, Michaleris P, Palmer TA (2015) Effect of inter-layer dwell time on distortion and residual stress in additive manufacturing of titanium and nickel alloys. J Mater Process Technol 215:123–131. https://doi.org/10.1016/j.jmatprotec.2014.07.030

[108] Han Q, Setchi R, Karihaloo B (2016) Challenges and Opportunities in the additive layer manufacturing of Al-Al₂O₃ nanocomposites. Impact J Innov Impact 8:389

[109] Tapia G, Elwany AH, Sang H (2016) Prediction of porosity in metal-based additive manufacturing using spatial Gaussian process models. Addit Manuf 12:282–290. https://doi.org/10.1016/j.addma.2016.05.009

[110] Tammas-Williams S, Withers PJ, Todd I, Prangnell PB (2016) The effectiveness of hot isostatic pressing for closing porosity in titanium parts manufactured by selective electron beam melting. Metall Mater Trans A Phys Metall

Mater Sci 47:1939–1946. https://doi.org/10.1007/s11661-0 16-3429-3

[111] Simchi A (2006) Direct laser sintering of metal powders: mechanism, kinetics and microstructural features. Mater Sci Eng, A 428:148–158. https://doi.org/10.1016/j.msea.2006. 04.117

[112] Kobryn PA, Moore EH, Semiatin SL (2000) Effect of laser power and traverse speed on microstructure, porosity, and build height in laser-deposited Ti-6Al-4V. Scr Mater 4:299–305. https://doi.org/10.1016/S1359-6462(00)00408-5

[113] Rahimian M, Ehsani N, Parvin N, Baharvandi H, Reza H (2009) The effect of particle size, sintering temperature and sintering time on the properties of Al-Al2O3 composites, made by powder metallurgy. J Mater Process Technol 209:5387–5393. https://doi.org/10.1016/j.jmatprotec.2009. 04.007

[114] Flom Y, Arsenault RJ (1989) Effect of particle size on fracture toughness of SiC/Al composite material. Acta Metall 37:2413–2423. https://doi.org/10.1016/0001-6160(89)90039-4

[115] Uddin SM, Mahmud T, Wolf C et al (2010) Effect of size and shape of metal particles to improve hardness and electrical properties of carbon nanotube reinforced copper and copper alloy composites. Compos Sci Technol 70:2253–2257. https://doi.org/10.1016/j.compscitech.2010. 07.012

[116] Wang Y, Shi J (2019) Engulfment and distribution of second-phase nanoparticle during dendrite solidification of an Al–Si binary alloy: a simulation study. Appl Phys A 125:449. https://doi.org/10.1007/s00339-019-2738-y